

Submarine landslide geomorphology, US continental slope

B.G. McAdoo^{a,*}, L.F. Pratson^b, D.L. Orange^c

^aVassar College, Department of Geology and Geography, Box 735, Poughkeepsie, NY 12604, USA

^bDivision of Earth and Ocean Sciences, Duke University, Durham, NC 27708-0227, USA

^cEarth Sciences Board, University of California, Santa Cruz, CA 95064, USA

Received 25 March 1999; accepted 13 March 2000

Abstract

The morphometric analysis of submarine landslides in four distinctly different tectonic environments on the continental slopes of Oregon, central California, Texas, and New Jersey provides useful insight into submarine process, including sediment transport mechanisms and slope stability. Using Geographic Information System (GIS) software, we identify landslides from multibeam bathymetric and GLORIA sidescan surveys based solely on surficial morphology and reflectivity. This method provides useful data in a time- and cost-efficient manner. We measure various aspects of the failures, including landslide area, runout distance, and headscarp height, along with the slope gradient of the runout zone, the failure's scar, headscarp, and adjacent slopes. The largest failures of the four study areas occur in the Gulf of Mexico, adjacent to Mississippi Canyon, and between salt withdrawal basins. Smaller landslides occur within the basins, and at the base of the Sigsbee Escarpment. These smaller landslides tend to have higher headscarps than the larger ones, and often have cohesive material at the base, suggesting a stronger rheology. Oregon has the steepest local slopes, but surprisingly few large failures for a seismically active margin (especially in the north), implying that slope angle and seismic activity may not be the most important slope stability controls. The California continental slope is heavily incised, which makes failure isolation difficult. Most of the landslides occur within the larger canyons (Vizcaino, Pioneer, Monterey) and adjacent to a pock mark field in the Point Arena basin. The majority of landslides offshore New Jersey occur on the open slope between Lindenkohl and Carteret Canyons.

Morphometric statistics give us insight into where mass movements occur, how big they are likely to be, their relative importance as sediment transport mechanisms, and the overall slope stability of a given margin. Most landslides occur on slopes less than 10°. Curiously, the steepness of the slope adjacent to the failure tends to be inversely proportional to the runout length. In both California and Oregon, slope failures tend to make the local slope steeper, whereas failures in the Gulf of Mexico and offshore New Jersey will tend to make the local slope less steep. Landslides with rubble beneath the scar are mostly smaller than those without, are deep seated, and make the slope steeper. We use the ratio of headscarp height to runout length as a measure of the failure's dynamic rheology. This ratio in the submarine case is orders of magnitude less than subaerial landslides. Hydroplaning of the failed mass may be responsible for the very long runout lengths. These morphometric relationships give us important insight into landslide dynamics and process in different sedimentary and tectonic environments. © 2000 Elsevier Science B.V. All rights reserved.

Keywords: Submarine landslides; Geomorphology; Mass movements; Multibeam bathymetry; Geographic information systems (GIS); Morphometric analysis

1. Introduction

Submarine landslides are an important mechanism in shaping and moving vast quantities of sediment

* Corresponding author.

E-mail address: brmcadoo@vassar.edu (B.G. McAdoo).

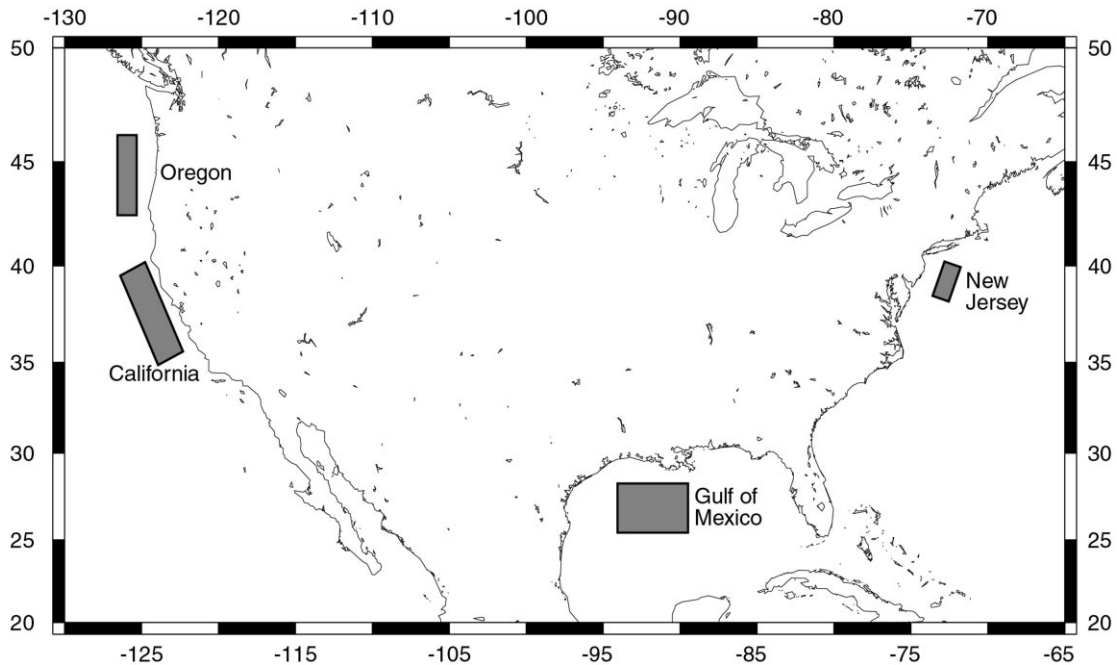


Fig. 1. Location of Oregon, California, Gulf of Mexico, and New Jersey study areas. Boxes outline approximate extents of NOAA multibeam bathymetric surveys.

down continental slopes on both active and passive margins. The largest documented submarine landslide, the Agulhas failure offshore South Africa, moved 20,000 km³ in one failure event (Dingle, 1977). A landslide/tsunami devastated Valdez and Seward, Alaska during the great 1964 Prince William Sound earthquake (Coulter and Migliaccio, 1966), and large storm waves associated with the 1969 Hurricane Camille triggered landslides which damaged three offshore oil platforms on the Mississippi Delta (Bea, 1971). Little work has been done on comparative morphology of failures within and between margins in different geologic settings. Isolating commonalities and differences of landslide morphology yields insight into the processes that shape a particular margin, and other margins with similar tectonic and sedimentary settings.

This study catalogs submarine landslides in four clastic environments within the United States Exclusive Economic Zone (US-EEZ), using sidescan sonar and multibeam bathymetric data, with the aim of finding where landslides occur, and what triggers them. We map failure scars on the actively

accreting continental slope off the convergent Oregon coast, a section of the transform fault-dominated central California margin, the salt tectonics province of the Gulf of Mexico, and a portion of the passive margin offshore New Jersey (Fig. 1). The contrasting sedimentary and tectonic provinces provide an interesting venue to compare landslide morphology. The resulting database contains statistical data on 83 mass flows, slides, and slumps.

By gaining an understanding of how submarine landslides look and where they occur, we can begin to infer what triggered these failures and when. Little is known about triggers of deepwater failures. Most are assumed to be seismically triggered because the continental slopes typically have gradients less than 5° (which would be statically stable, unless and unreasonably weak sediment were involved), and are well below storm wave base where cyclic loading might be an issue (Lee and Edwards, 1986; Lee et al., 1993). Using the morphology of the failure's location along with the present-day tectosedimentary environment, we can speculate on possible timing and triggering mechanisms of the landslides.

2. Methods

Booth et al. (1993) characterized submarine landslides on the US Atlantic continental slope between Massachusetts and North Carolina, however this is the first study that describes the similarities and differences in failure morphology between various tectonic regimes. We use gridded multibeam bathymetry from the National Oceanic and Atmospheric Administration (Grim, 1992), and GLORIA (Geological Long-Range Inclined Asdic) side-scan sonar to identify failures in the four study areas (EEZ-SCAN 87, 1991). Fig. 2a–d show the gridded multibeam data with landslides outlined in white.

Gridded at 100 m, the bathymetry data are capable of resolving discrete landslides greater than $\sim 1 \text{ km}^2$, tremendous by subaerial standard (Keefer, 1984; Dade and Huppert, 1998), but not very large on a continental margin-wide scale. The location of the NOAA soundings have an areal accuracy within $< 50 \text{ m}$, and the vertical resolution is $< 1\%$ of water depth (Grim, 1992). The GLORIA system uses high-frequency sound waves to record seafloor acoustic impedance. The GLORIA data are gridded with 50 m wide cells, and is also capable of identifying landslides $> 1 \text{ km}^2$ (Fig. 3).

2.1. Slide determination

To locate the slope failures, we combine the bathymetry and GLORIA data using a Geographical Information System (GIS) software package. Landslides are initially identified using the bathymetry (so that we can make the morphometric measurements) and bolstered using the side-scan data. Overlaying the bathymetry data with the GLORIA data presents the challenge of fitting a two-dimensional image over a three dimensional surface. We overcome this obstacle by focussing in on small regions and using the GIS to shift the image such that the reflectivity agrees with

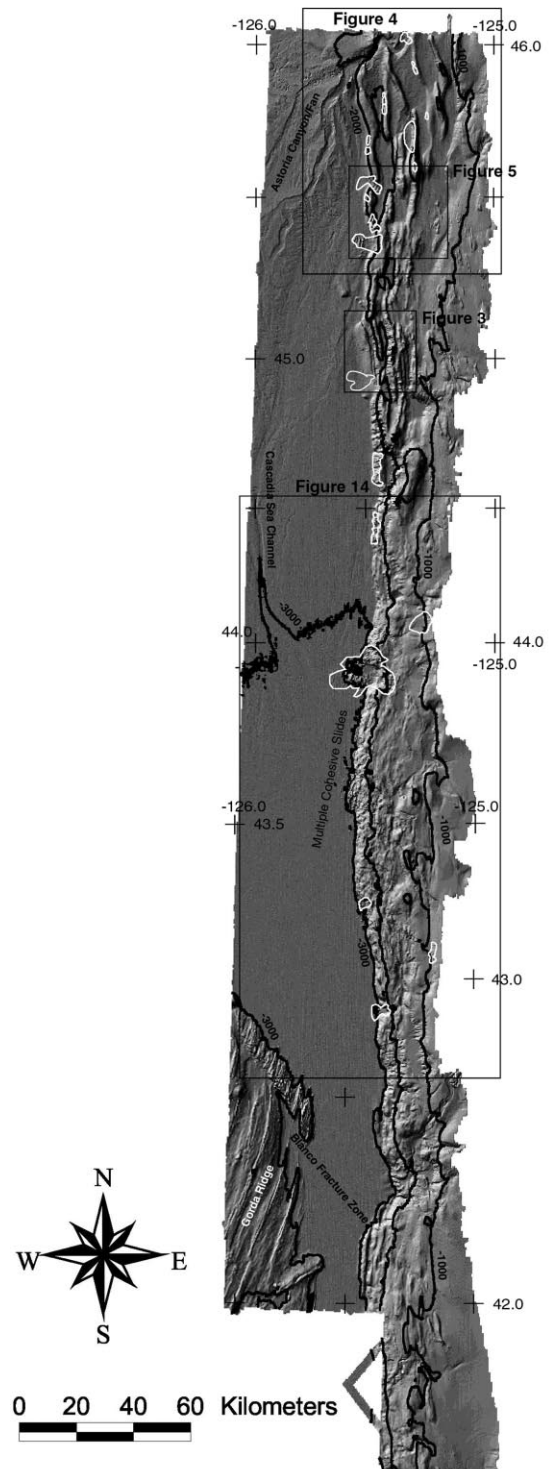


Fig. 2. a–d. Gridded NOAA multibeam bathymetric data of the four study areas. Shaded bathymetry maps have a sun illumination angle with an azimuth of 315° and a 65° inclination. Slides are outlined in white, with 1000 m contours in black. Boxes indicate the extents of following figures. (a) Oregon Margin, (b) California Margin, (c) Gulf of Mexico, (d) New Jersey Margin.

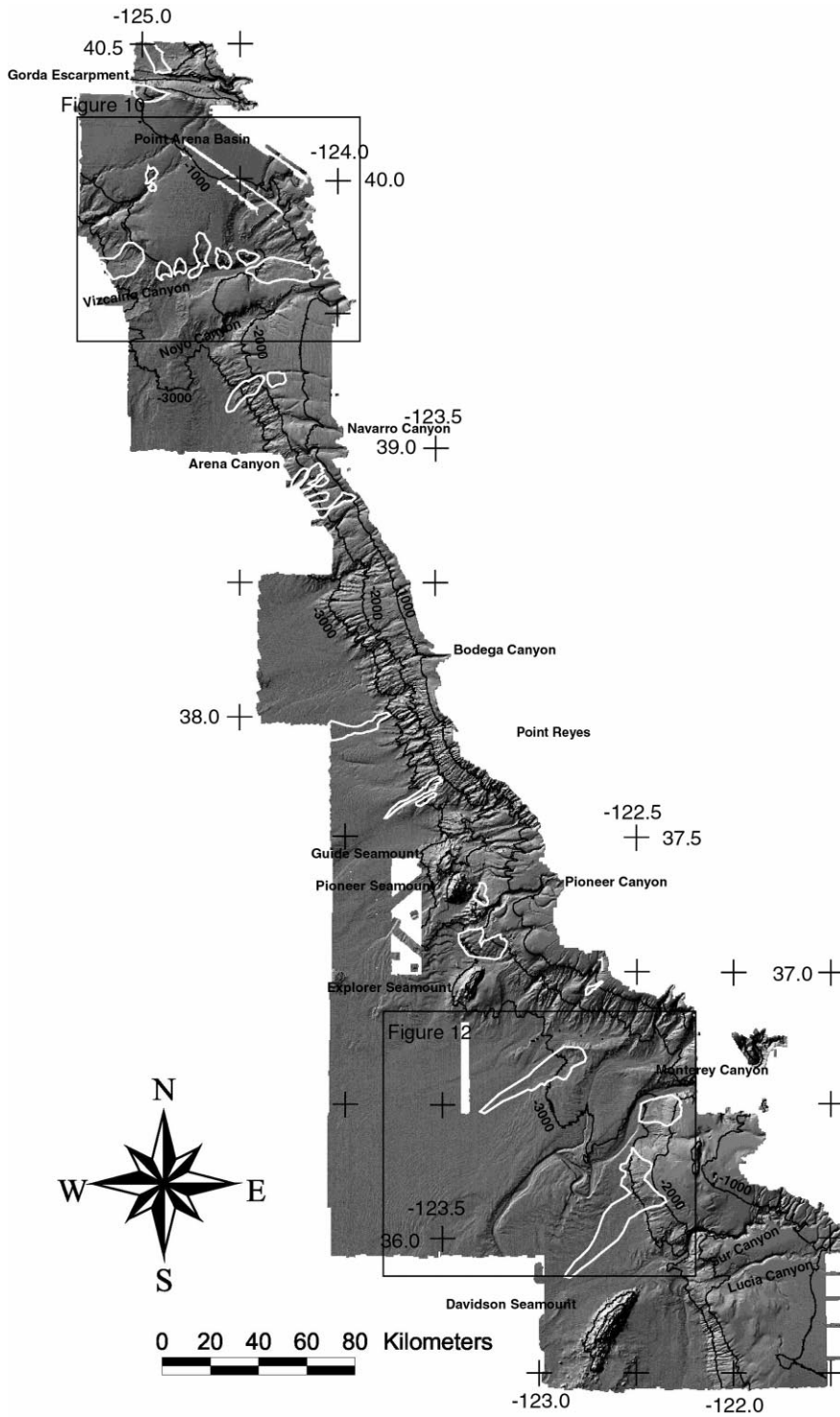


Fig. 2. (continued)

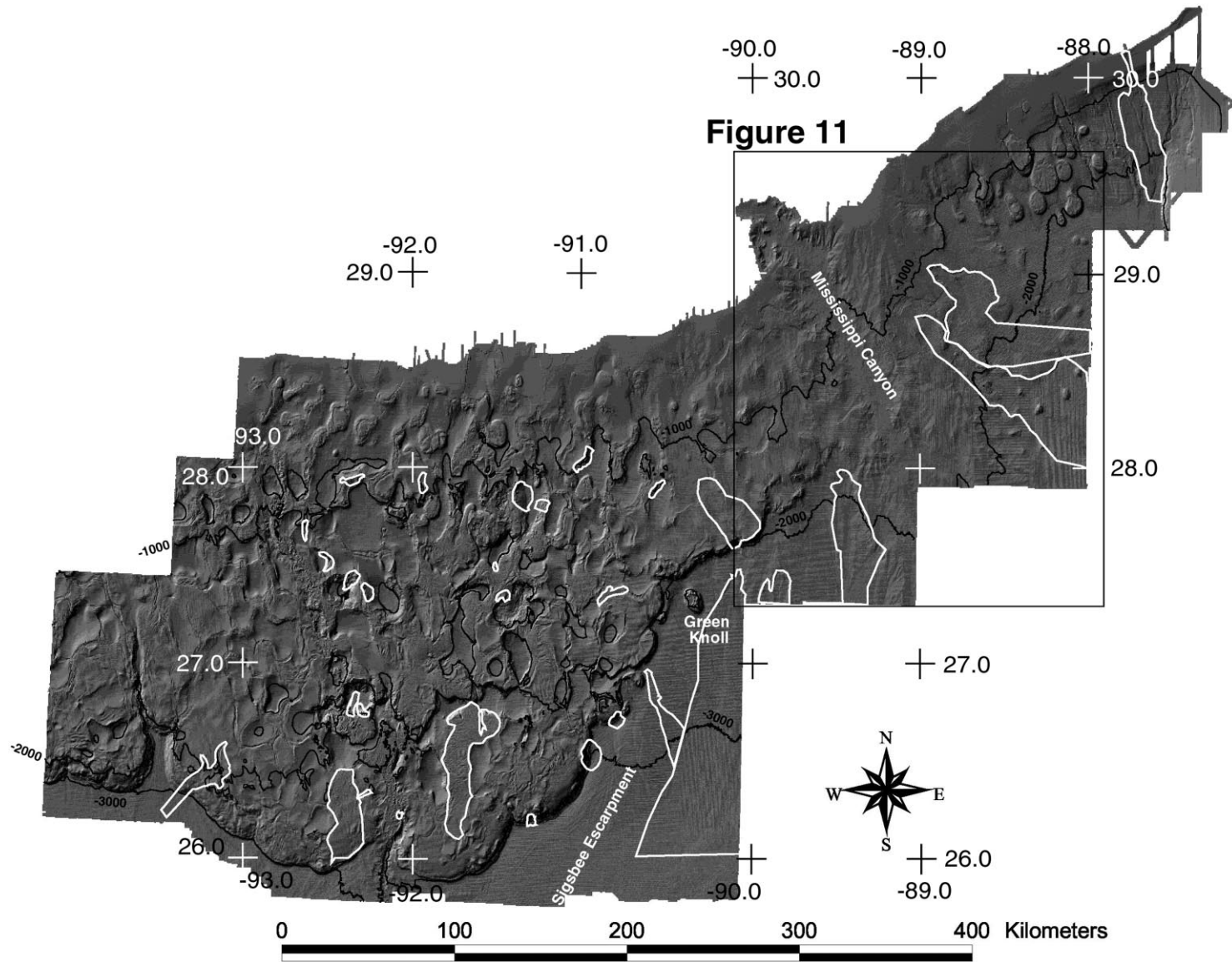


Fig. 2. (continued)

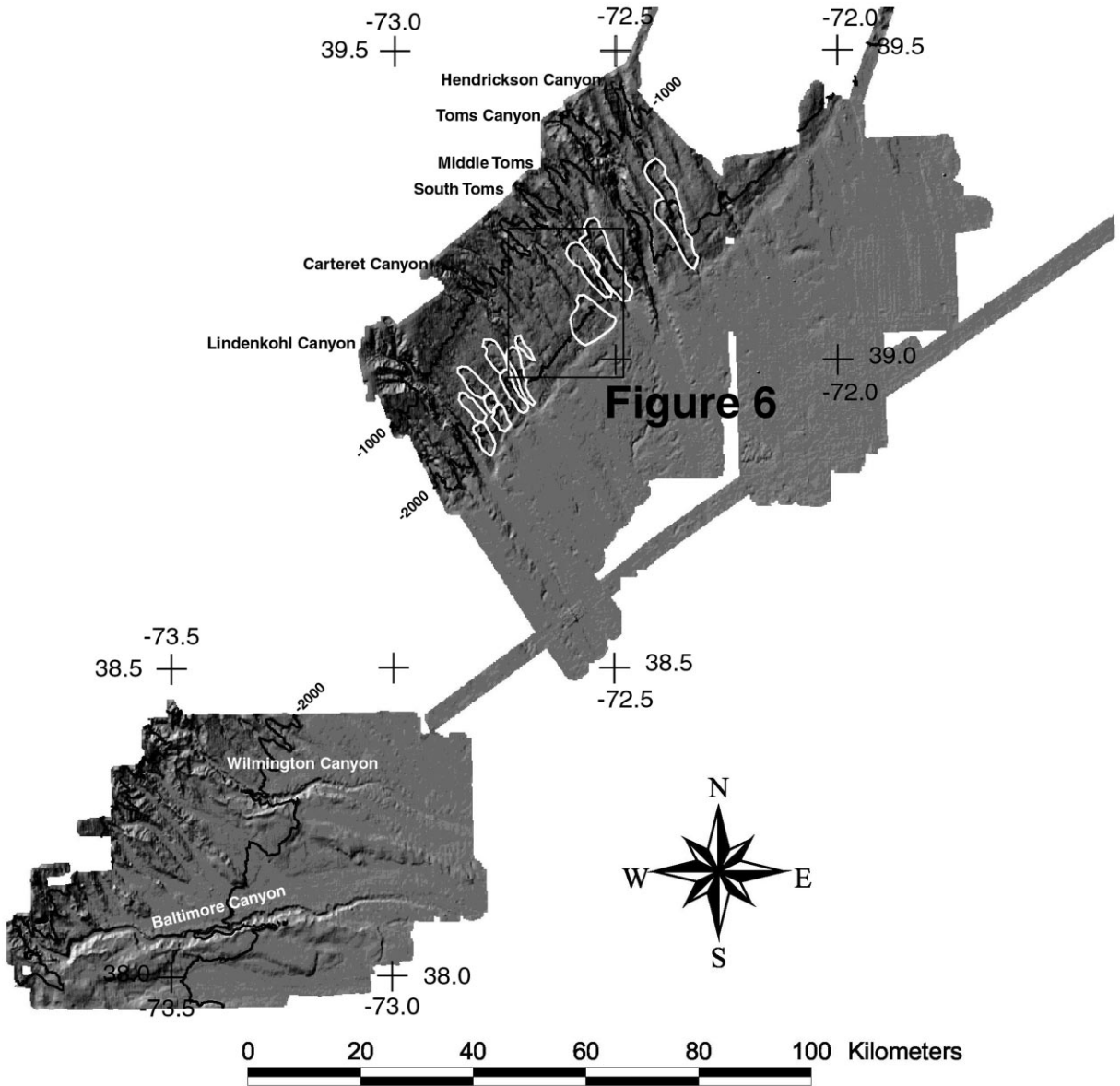


Fig. 2. (continued)

bathymetric observations on a small scale (e.g. lining up a band of high reflectivity with a steep slope).

Once a small area is georeferenced, we use maps created in the GIS to identify areas of rapid changes in slope gradient with the shape of an arcuate headscarp with extending sub-parallel sidewalls. An artificial hillshading subroutine illuminates bathymetric roughness, such as steep headscarps and sidewalls,

and sometimes rubble at the base of the landslide scar. Another subroutine creates slope maps that illuminate regions of consistently steep slopes by computing a mean value for one grid cell from the slope gradient between it and the eight neighboring grid cells. Slope maps clearly image the diagnostic short wavelength changes in bathymetry associated with arcuate headscarps and connected sidewalls

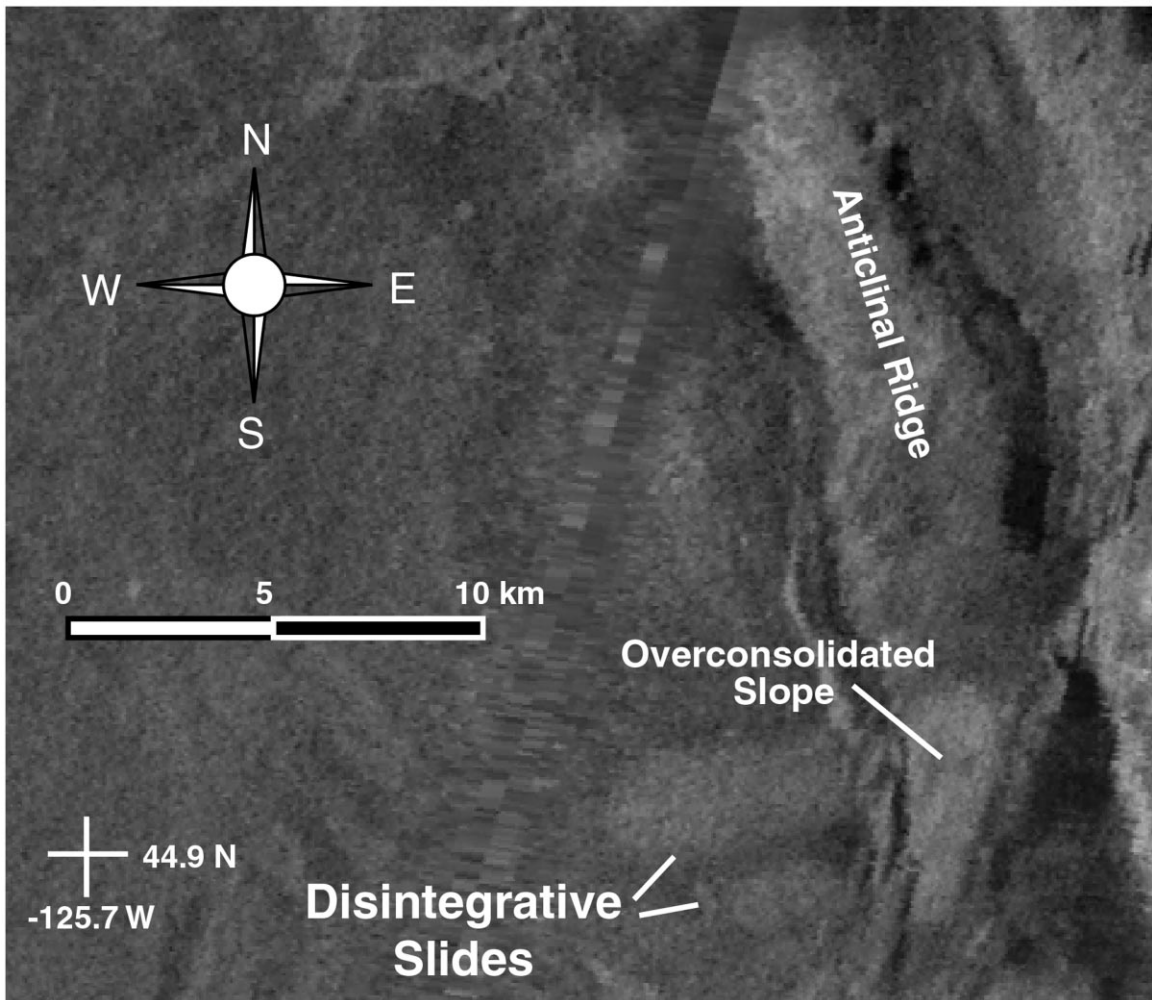


Fig. 3. GLORIA image of the base of the Oregon continental slope. High reflectivity lobes indicate failure deposits. The high reflectivity zone east of the lobes is most likely due to eroded, overconsolidated sediment. The anticlinal ridge is also higher reflectivity due to the higher incidence angle of the sonar signal.

(Fig. 4). We exclude canyons and other erosive features (including regions that possibly have multiple superimposed failure scars) which lack the diagnostic arcuate headscarp.

There are several known shortfalls of this method. (1) There are undoubtedly numerous older and shallow-seated failures that we simply missed because they lack a significant bathymetric signature. (2) While the cumulative effects may be substantial, we have not documented landslides less than 1 km^2 in size. (3) There could be zones of overlapping failures expressed as rough seafloor that we did not pick

because we could not clearly identify a headscarp. (4) Because we use only surface data (no reflection seismic data), the data will be biased towards the more recent failures, which will have unknown effects on the quantitative and qualitative interpretations of the data. All of these features might be obvious in sub-bottom profiles and/or higher resolution data. However, this method has the distinct advantage of allowing us to use existing, publicly available datasets to quantify landslide morphologies and make comparisons between geographically diverse environments (including subaerial digital elevation models).

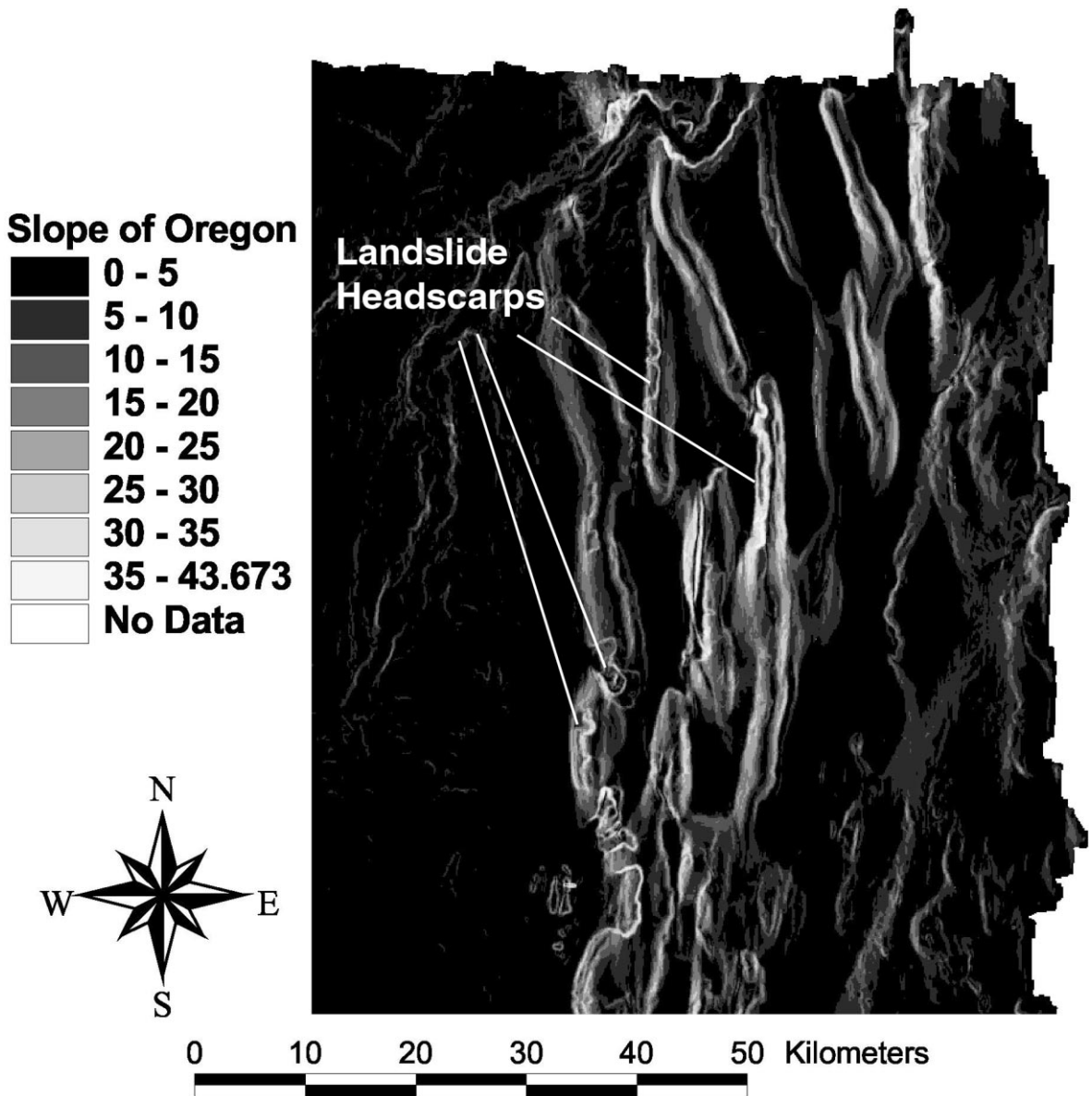


Fig. 4. Oregon slope gradient map. Grayscale values in the legend on the left are in degrees. White represents higher slope gradients. Note well-imaged arcuate headscarps and canyon walls.

2.2. Terminology

It is difficult to determine whether a mass movement is a slump, debris flow, rockfall, etc. based solely upon surficial morphology. Thus the terms used here refer to the state in which the material appears on the seafloor at present. “Landslide” or

“slope failure” refers to an area of disturbed seafloor caused by the downslope movement of a failed mass. The terms “blocky” and “cohesive” describe failures with rubble present at the base of the eroded seafloor, interpreted to be allochthonous material from the failure (Hampton et al., 1996). “Disintegrative” refers to landslides that have no obvious landslide mass at or

near the base of the scar. The landslide mass either lost cohesion during failure (e.g. debris flow; Booth et al., 1993), failed as a cohesive mass, and disintegrated over time, or may have been buried by subsequent sedimentation (either hemipelagic or other slope failures). Thus a failure that may have had cohesive rubble at its base that has been eroded over time so there is no longer a bathymetric expression would be classified as disintegrative under this scheme. Fig. 5 shows examples of both disintegrative and blocky landslides. A “slump” is a cohesive landslide where the failed mass rotates along a curved slip surface, and the failed material does not exceed the downslope limit of the scar (Lee et al., 1993; Fig. 6). In areas of thin sediment cover, bathymetric highs have often been misinterpreted in seismic profiles as allochthonous blocks, before they were shown to be part of the oceanic crust (Heezen and Drake, 1964; Hughes-Clarke, 1990). In this study, however, most of the blocky material rests on flat, sedimented basin floors where other forms of angular material are highly unlikely.

2.3. Measurements

Once the failures are categorized, we measure the headscarp’s depth and height from the bathymetry data and, using a combination of the bathymetry and GLORIA data, the total area of seafloor affected by the failure, and runout distance (where identifiable). The headscarp region is the steepest slope in the eroded scar zone (Fig. 5f). There is usually variation in height across the headscarp, therefore, we use a mean value calculated from numerous cross-sections (Fig. 7). In the case of failures (especially slumps) where the headscarp cannot be easily distinguished from the scar, the headscarp height is measured as the steepest measurable section within the failure scar (Fig. 6). The failure area is defined as the portion of seafloor with anomalous bathymetry and/or reflectivity consistent with our identification criteria described above (headscarp, sidewalls, rubble or anomalous reflectivity at the base—the shaded regions in the inset of Fig. 5a and d). Where there is no evidence of the landslide mass in the runout zone (i.e. no irregular bathymetry or reflectivity), the area includes the scar, headscarp, and sidewalls only, and is a minimum (Fig. 5a). When the area of disturbed

seafloor exceeds the limits of our data, the area is likewise a minimum. Runout distance is the limit of the disturbed seafloor downslope of the failure’s headwall (dashed line in Fig. 5a). In the case of blocky landslides, the runout corresponds to the distance of the furthest piece of cohesive debris (Fig. 5c) from the headscarp (Fig. 5f). We use the GLORIA data to determine the runout distance of disintegrative landslides. The runout is the distance from the headscarp to the furthest edge of the anomalous reflectivity, or the end of the sidewalls if no discernable reflectivity is present (Fig. 5a).

We measure slope gradients from the GIS slope maps. Runout, scar, and headscarp slope angles, along with the slope gradient adjacent to the scar, are calculated using an average of numerous individual cells (the number is dependent on the available area for each factor). We assume that the gradient of the unfailed slope immediately adjacent to the failure (but at least 1 grid cell [100 m] away) is a close representation of the seafloor prior to slope failure.

We calculate the landslide volume (V_{slide}) by using the thickness ($T = h \cos \alpha$, where h is the headscarp height, and α the scar slope angle) and area, and then model the volume as a wedge geometry

$$V_{\text{slide}} = 1/2(A_s)(h \cos \alpha)$$

where A_s is the area of the scar (Fig. 8). All data are compiled in Table 1.

3. Results

3.1. Landslide location

The evidence of slope failure is widespread on each of the four margins. The convergent Oregon margin lacks numerous steep-walled canyons, and is dominated by steep local slope gradients associated with the Cascadia accretionary prism (Fig. 2a). The California continental slope is steep (but not as steep as Oregon [Pratson and Haxby (1996)]) and rough, but is cut by several major, steep-walled canyons (north to south: Vizcaino, Pioneer, Ascension/Año Nuevo, and Monterey) and small, unnamed canyons too numerous to count (Fig. 2b). Tectonics associated with the mobile salt layer that underlies the continental slope offshore Texas

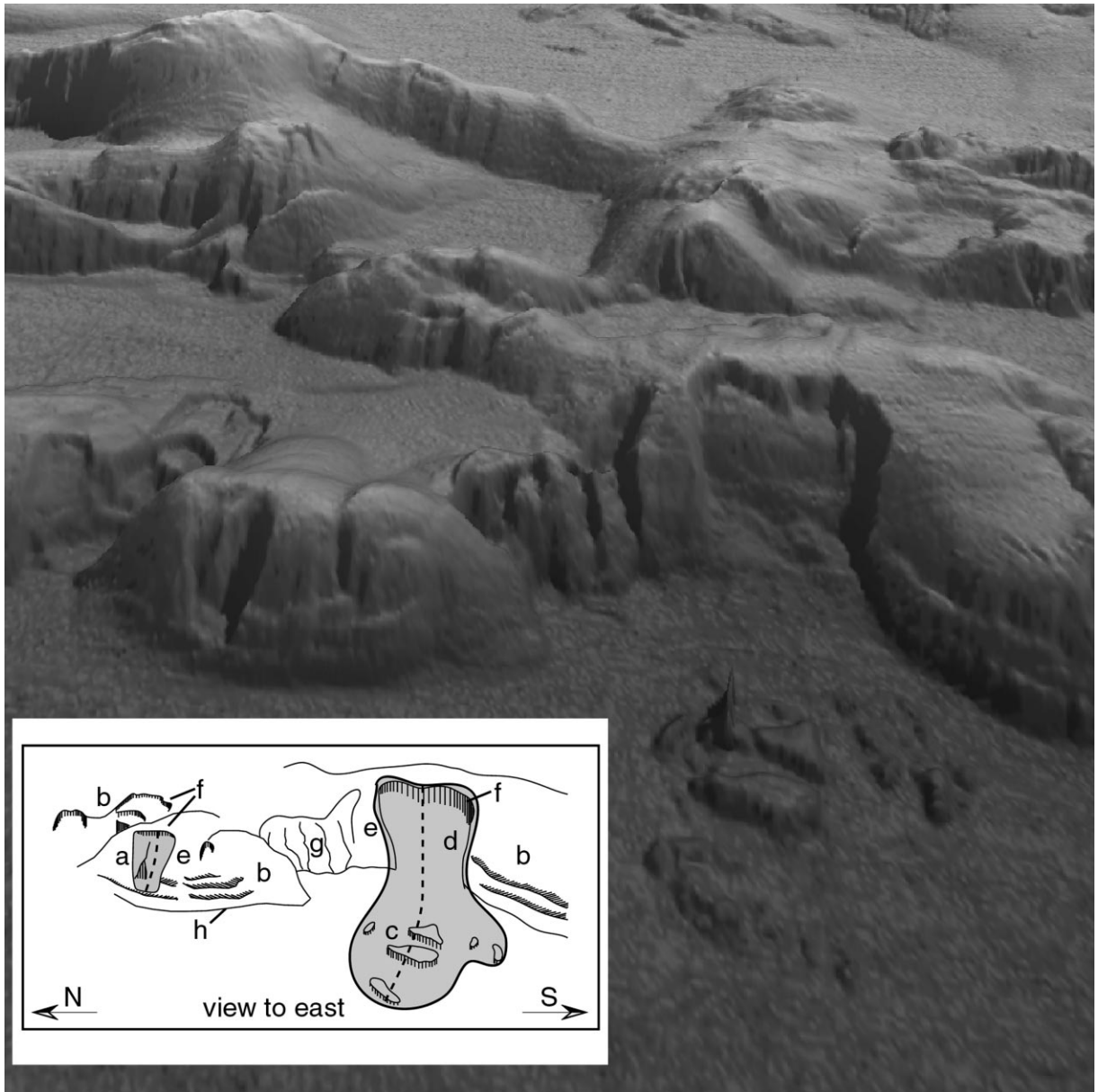


Fig. 5. Three-dimensional perspective image of the base of the Oregon continental slope, approximately $3\times$ vertical exaggeration. View is looking east; north is to the left. Scale varies with distance in the perspective, however the field of view at the slope base is approximately 30 km. Inset is a line drawing of figure, with labels (a to h) referred to below. Disintegrative landslides (a and b) have characteristic scar morphology, but lack bathymetric evidence of failed material at the base of the failure. The slope failure deposits for cohesive landslides (c) are associated with a particular scar directly up gradient (d). The gray shaded regions represent the measured landslide area, and the dashed lines the runout distance. The angle of the unfailed slope adjacent to the failure scar (e) is used as a proxy for the pre-failure slope gradient. Landslide headscarps (f) are the steep upslope regions at the top of the scar. “Eroded slope” (g) refers to regions of the seafloor where material has been removed, however no evidence of discrete landslide events (i.e. a distinct headscarp) is present. A series of curious terraces (h) rim the very base of the slope, and often coincide with the lowermost terminus of the landslides, resulting in a “Hanging Slide” (a). Notice the seafloor with little visible evidence of erosion between landslide scars on the westernmost ridge (closest) and on the other background ridges.

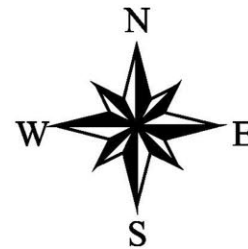
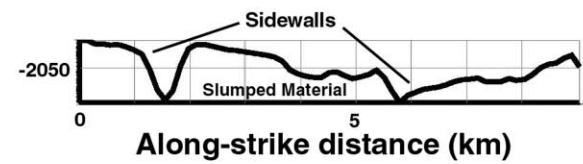
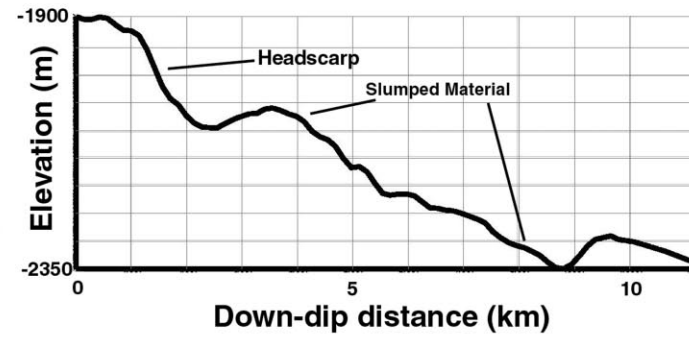
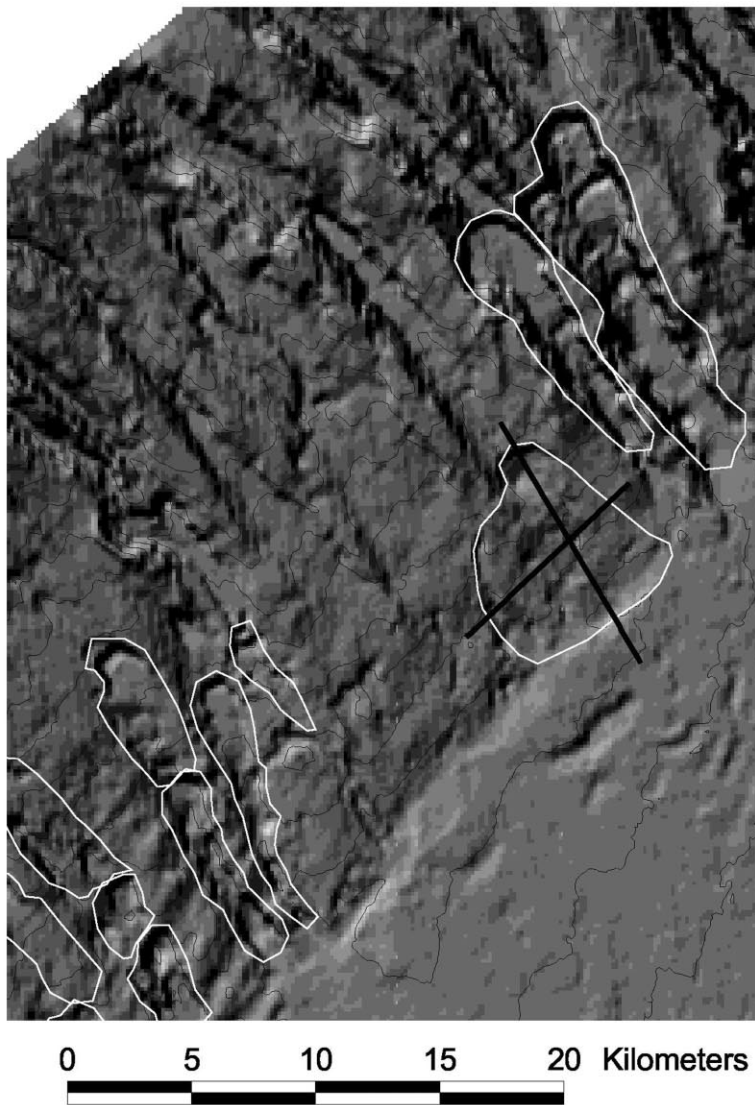


Fig. 6. Shaded relief map and cross-sections of a small slump on the New Jersey continental slope (see Fig. 2d for location). Sun illumination angle is 65° with an azimuth of 315° . The two bold lines in the shaded relief map are the dip and strike cross-sections. Both cross-sections have a vertical exaggeration of $10\times$. The upper section is a NW-SE dip section through the slump that shows the headscarp and the mass of the slumped material. The lower inset is a SW-NE strike section that shows the slump's sidewalls and the slumped material.

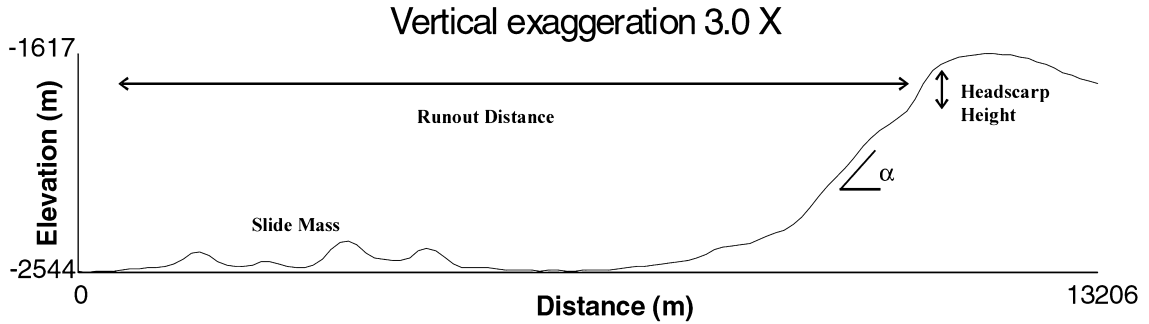


Fig. 7. Cross-section through the cohesive landslide on Oregon's lower continental slope shown in Fig. 5. Vertical exaggeration is $\sim 3 \times$. The failed mass shows up as irregular bathymetric highs downslope from the scar. The headscarp is the steepest slope gradient within the scar. The runout distance is measured from the top of the headscarp to the furthest extent of disturbed (eroded or deposited) seafloor. The slope within the scar (α) is calculated as an average through several cross-sections and points on the slope map.

produces locally steep regions around diapirs and basins (Twichell and Delorey, 1996; Fig. 2c). Mississippi Canyon is a major feature with diffuse bathymetry and very large failures nearby. As in California, numerous canyons cut the passive New Jersey margin creating a rough appearance on a shallow overall slope (Pratson and Haxby, 1996; Fig. 2d). The New Jersey margin also has a unique lithology of Eocene chalk that creates steep slopes susceptible to failure (McHugh et al., 1993).

The Oregon margin can be separated into two different structural regimes: North of 44.85° faults and folds of the prism show dominantly landward vergence, and south of 44.85° , structures tend to

verge seaward (Goldfinger et al., 1992; MacKay, 1995), and the two regimes exhibit a different landslide style. Ten of the 12 landslides are disintegrative in the north while six of seven of the southern landslides are cohesive (Fig. 9). The regional gradient of the continental slope is steeper in the south where the margin is narrower (~ 20 vs. ~ 40 km in the landward vergent region). The seafloor in the region of landward verging structures tends to be smooth, whereas the seafloor in the seaward verging structural region has a very rough appearance (Fig. 2a). All landslides north of 44.85° occur on the flanks of the anticlines (except one blocky landslide on an inside meander of Astoria Canyon), and in the seaward verging section

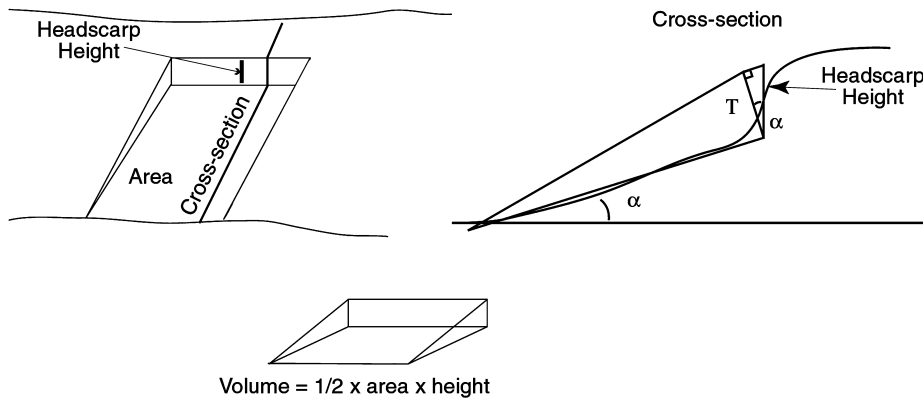


Fig. 8. Schematic diagram of volume calculation. We measure landslide area, headscarp height, and scar slope from the GIS maps. Using these data, we calculate an approximate volume of seafloor excavated by assuming a wedge-shaped geometry. Generally, erosion decreases downslope, resulting in sidewalls that are equal in height to the headwall, decreasing to zero at the base where erosion diminishes, and deposition may begin. The volume is then the area of the landslide multiplied by the height, then divided by two to account for the wedge shape.

Table 1

Landslide statistics summary. Measured values include latitude, longitude, area, depth to the failures' headscarp (in meters), and length of runout. Headscarp, scar, runout, and local unfailed adjacent slope gradients, along with headscarp heights are calculated by taking the mean of numerous individual measurements. Volume is approximated using the landslide's thickness and area in a wedge geometry

Area	Latitude	Longitude	Type	Area (sq. km)	Depth of headscarp (m)	Runout (HS to toe) (km)	Headscarp slope (degrees)	Headscarp standard deviation	Scar slope (degrees)	Scar standard deviation	Unfailed adj. slope (degrees)	Adjacent standard deviation	Runout slope (degrees)	Runout standard deviation	Headscarp height (m)	Headscarp standard deviation	Slide volume (cubic km)	HS/RO (D/L) (unitless)	Volume (cubic km)
Oregon	46	-125.36	Blocky	10	-1494	4.2	10.5	1.5	6.2	2.9	15.7	8.8	3.9	0.8	49.3	1.0	0.2	0.012	0.2
	45.92	-125.35	Disint.	1	-1375	0.8	18.0	2.1	14.6	1.8	14.0	1.9	0.9	0.6	40.0	0.0	0.0	0.050	0.0
<i>n</i> = 20	45.9	-125.33	Disint.	3	-1356	1.3	19.4	3.1	11.6	2.5	14.0	1.9	0.9	0.6	90.0	0.0	0.1	0.069	0.1
	45.8	-125.47	Disint.	8	-1624	1.5	24.3	3.7	12.6	4.4	17.2	7.3	1.8	1.3	83.8	3.9	0.2	0.056	0.3
Total area: 18,430	45.77	-125.27	Disint.	2	-1424	0.9	17.5	1.5	11.2	2.7	12.1	3.3	1.2	0.9	37.5	3.5	0.0	0.042	0.0
	45.69	-125.34	Disint.	32	-1268	3.9	31.4	4.3	15.7	6.1	23.4	8.2	1.6	0.8	410.0	62.8	4.2	0.105	6.3
	45.64	-125.54	Disint.	3	-1901	1.4	23.8	3.1	10.2	2.2	16.9	6.5	1.3	0.6	184.0	11.1	0.2	0.131	0.3
% of Area w/slides	45.63	-125.33	Disint.	5	-837	n/a	3.1	2.4	12.2	2.4	10.9	3.3	n/a	n/a	11.3	1.2	0.0	0.000	0.0
3.0	45.53	-125.5	Disint.	27	-1809	10.0	22.8	5.0	10.3	2.4	16.5	4.5	1.0	0.6	82.4	7.9	0.7	0.008	1.1
	45.49	-125.5	Disint.	4	-1809	2.3	22.9	1.8	10.3	2.7	20.9	4.2	1.9	0.8	31.7	12.6	0.0	0.014	0.1
	45.49	-125.53	Disint.	7	-1522	6.0	27.9	2.4	10.2	5.3	19.8	6.3	1.7	1.3	102.5	3.5	0.2	0.017	0.4
	45.41	-125.5	Disint.	21	-1904	3.1	27.4	7.5	12.5	6.4	15.4	4.1	2.9	1.8	170.0	51.0	1.2	0.055	1.7
	45.36	-125.47	Blocky	48	-1626	10.0	27.6	4.5	17.9	5.6	15.4	4.1	1.2	1.3	186.7	30.6	2.8	0.019	4.3
	44.66	-125.42	Slump	30	-2008	2.9	30.8	5.6	28.3	6.9	21.1	4.4	1.4	1.0	408.3	14.4	3.6	0.141	5.4
	44.26	-125.44	Slump	21	-1810	2.1	32.9	4.8	33.0	4.5	21.5	6.8	1.5	1.3	368.8	94.4	2.1	0.176	3.2
	44.17	-125.2	Disint.	39	-549	8.7	22.9	5.6	14.2	4.6	14.9	4.0	3.2	1.4	137.5	20.2	1.7	0.016	2.6
	44	-125.39	Blocky	239	-1608	22.0	22.2	8.8	8.8	5.9	12.8	6.0	0.8	0.5	360.0	29.4	28.1	0.016	42.5
	43.27	-125.43	Blocky	13	-2924	4.4	28.6	5.6	18.3	5.1	18.1	7.7	1.2	2.4	346.7	25.2	1.4	0.079	2.1
	43.14	-125.44	Disint.	13	-717	2.4	14.1	1.4	10.0	3.6	7.6	1.3	1.7	0.6	53.6	9.6	0.2	0.022	0.3
	42.93	-125.34	Blocky	24	-2745	6.6	31.0	5.6	21.1	4.9	18.7	4.1	0.6	0.3	398.3	63.3	2.9	0.060	4.5
Mean	45.0	-125.4		27.4	-1615.5	5.0	23.0		14.5		16.3		1.6		177.6		2.5	0.054	total
Standard deviation	1.0	0.1		51.6	574.8	5.1	7.6		6.6		3.9		0.9		146.3		6.2	0.050	75.6
Median	45.5	-125.4		13	-1616	3.1	23.3		12.3		16.1		1.4		120.0		0.5	0.046	
California	40.41	-124.89	Disint.	71	-1971	15	20.2	4.4	10.7	4.1	4.2	1.9	1.5	0.7	137.5	3.5	3.2	0.009	4.8
	40.01	-124.93	Slump	21	-1347	5.6	9.6	3.6	3.0	1.2	2.2	0.6	5.6	1.9	80.0	15.0	0.6	0.014	0.8
<i>n</i> = 25	39.96	-124.92	Slump	6.8	-1513	2.7	11.6	3.1	11.6	3.1	1.5	1.0	5.6	1.9	71.3	16.8	0.2	0.026	0.2
	39.73	-124.66	Disint.	78	-1361	21	8.0	3.9	3.1	1.7	2.7	1.3	1.8	0.7	167.5	10.6	4.3	0.008	6.5
Total area: 32,930	39.73	-124.97	Disint.	159	-2163	17	14.4	3.1	6.3	1.9	7.9	1.8	3.4	1.7	192.5	51.2	10.0	0.011	15.2
	39.71	-124.58	Disint.	36	-1665	8.2	12.9	5.2	6.6	2.8	2.8	0.6	1.5	0.5	201.7	7.6	2.4	0.025	3.6
	39.66	-124.21	Disint.	208	-825	26	11.5	3.8	3.2	1.9	2.2	0.7	1.8	1.1	65.3	2.5	4.5	0.003	6.8
% of Area w/slides	39.69	-124.47	Slump	34	-1715	7.9	9.3	3.6	9.3	3.6	3.0	2.4	1.8	1.0	233.3	77.7	2.6	0.030	3.9
7.1	39.68	-124.77	Disint.	22	-2355	5.4	6.4	2.1	5.8	1.6	3.3	0.9	2.4	1.4	45.0	5.0	0.3	0.008	0.5
	39.67	-124.86	Disint.	28	-2157	5.7	6.4	1.7	6.3	2.6	3.1	0.9	2.6	1.4	80.0	0.0	0.7	0.014	1.1
	39.26	-124.26	Disint.	95	-1854	21	15.9	4.2	6.2	3.6	5.0	1.6	3.1	2.7	101.3	15.5	3.2	0.005	4.8
	39.25	-124.37	Slump	35	-2233	7.1	10.7	2.1	2.9	1.4	4.6	1.9	2.7	1.6	76.7	14.4	0.9	0.011	1.3
	38.89	-124.17	Disint.	25	-1688	9	18.3	5.2	7.0	4.7	5.0	2.7	n/a	n/a	120.0	10.0	1.0	0.013	1.5
	38.89	-124.13	Disint.	62	-1424	12	18.4	4.6	6.2	2.4	5.0	2.7	n/a	n/a	146.7	17.5	3.0	0.012	4.5
	38.88	-124.09	Slump	30	-1196	8.9	9.1	2.2	9.1	2.2	3.8	1.9	n/a	n/a	75.0	10.0	0.7	0.008	1.1
	38.69	-123.89	Slump	42	-1462	17	18.8	3.0	6.0	3.9	5.4	1.4	n/a	n/a	100.0	26.5	1.4	0.006	2.1
	38	-123.77	Disint.	107	-2105	26	17.1	4.2	2.0	0.9	4.0	0.5	n/a	n/a	130.0	0.0	4.6	0.005	7.0
	37.75	-123.55	Disint.	56	-2613	28	27.0	7.8	8.5	4.3	7.3	2.7	1.0	0.4	200.0	49.5	3.7	0.007	5.5
	37.7	-123.54	Disint.	17	-2717	9.1	27.5	5.4	4.4	3.3	8.3	2.9	3.9	1.2	216.7	2.9	1.2	0.024	1.8
	37.33	-123.32	Disint.	33	-1557	6.7	15.2	4.4	8.3	3.5	5.5	1.4	5.3	1.9	111.3	21.7	1.2	0.017	1.8
	37.14	-123.32	Disint.	167	-2160	11	16.9	4.8	5.7	1.9	n/a	n/a	3.0	2.5	113.3	60.1	6.2	0.010	9.4
	36.99	-122.76	Disint.	12	-835	8.6	8.8	0.5	4.8	1.1	5.3	1.2	7.6	4.3	30.0	0.0	0.1	0.003	0.2
	36.71	-122.85	Disint.	295	-2585	48	9.8	2.6	3.5	3.0	2.6	1.7	1.1	0.4	82.5	14.4	8.0	0.002	12.1
	36.52	-122.44	Disint.	167	-1781	16	13.2	3.2	6.6	1.0	n/a	n/a	1.5	1.0	113.3	25.5	6.2	0.007	9.4
	36.24	-122.54	Disint.	525	-2429	51	14.1	5.8	6.3	1.9	4.6	1.2	1.0	0.6	105.8	62.5	18.2	0.002	27.6
Mean	38.7	-124.0		93.3	-1828.4	15.8	14.0		6.1		4.3		2.9		119.9		3.5	0.011	total
Standard deviation	1.3	0.8		115.2	523.7	12.4	5.6		2.5		1.8		1.8		55.0		4.0	0.008	133.7
Median	38.9	-124.2		42	-1781	11	13.2		6.2		4.2		2.5		111.3		2.6	0.009	

Table 1 (continued)

Area	Latitude	Longitude	Type	Area (sq. km)	Depth of headscarp (m)	Runout (HS to toe) (km)	Headscarp slope (degrees)	Headscarp standard deviation	Scar slope (degrees)	Scar standard deviation	Unfailed adj. slope (degrees)	Adjacent standard deviation	Runout slope (degrees)	Runout standard deviation	Headscarp height (m)	Headscarp standard deviation	Slide volume (cubic km)	HS/RO (D/L) (unitless)	Volume (cubic km)
Oregon	46	-125.36	Blocky	10	-1494	4.2	10.5	1.5	6.2	2.9	15.7	8.8	3.9	0.8	49.3	1.0	0.2	0.012	0.2
	45.92	-125.35	Disint.	1	-1375	0.8	18.0	2.1	14.6	1.8	14.0	1.9	0.9	0.6	40.0	0.0	0.0	0.050	0.0
Gulf of Mexico	26.25	-93	Disint.	452	-1918	49	8.7	1.9	1.0	0.7	1.1	0.6	1.0	0.3	60.0	0.0	8.9	0.001	13.6
	27.42	-92.49	Slump	44	-1423	3.8	13.6	1.8	5.8	2.1	2.1	0.8	1.4	1.0	140.0	7.1	2.0	0.037	3.1
<i>n</i> = 25	27.39	-92.37	Disint.	29	-1469	12	8.3	1.2	3.3	1.3	3.0	1.0	0.9	0.4	111.7	44.8	1.1	0.009	1.6
	27.4	-92.27	Slump	62	-1356	12	13.5	2.8	4.9	2.2	3.1	0.6	2.7	1.1	148.3	7.6	3.0	0.012	4.6
Total area: 61,670	27.3	-92.19	Disint.	48	-1301	5.5	9.7	2.1	4.3	1.4	5.5	2.1	7.6	1.1	75.0	7.1	1.2	0.014	1.8
	26.67	-92.26	Disint.	52	-2024	14	16.2	3.4	2.8	1.4	5.0	2.2	1.8	1.0	200.0	0.0	3.4	0.014	5.2
% of Area w/slides 26.9	26.67	-92.19	Blocky	15	-1874	8.8	17.2	3.1	7.5	4.0	11.5	2.7	1.0	0.4	160.0	0.0	0.8	0.018	1.2
	26.28	-92.14	Disint.	15	-2053	8.6	8.1	1.6	2.5	1.0	1.1	0.8	1.0	0.5	110.0	17.3	0.5	0.013	0.8
26.9	26.36	-91.98	Disint.	10.3	-2019	3	16.0	0.9	5.1	3.0	6.0	3.6	n/a	n/a	203.3	5.8	0.7	0.068	1.0
	26.74	-91.61	Disint.	1156	-2150	79	15.9	3.8	0.9	0.5	n/a	n/a	n/a	n/a	263.3	100.2	100.4	0.003	152.2
26.9	27.29	-91.41	Blocky	9.6	-1757	4.9	15.2	4.0	8.6	2.9	12.0	3.7	1.8	0.7	160.0	0.0	0.5	0.033	0.8
	27.11	-91.41	Disint.	34	-1733	7.6	8.9	2.3	2.1	1.5	2.5	1.2	1.7	1.8	60.0	0.0	0.7	0.008	1.0
26.9	27.94	-91.32	Blocky	143	-1076	12	14.7	4.1	6.0	7.3	5.0	3.1	1.2	0.5	176.3	73.4	8.3	0.015	12.5
	26.21	-91.19	Disint.	28	-2399	7.3	17.3	1.3	7.2	3.8	5.1	1.0	1.0	0.7	191.7	2.9	1.8	0.026	2.7
26.9	27.79	-91.18	Blocky	42	-1332	6.8	13.1	3.2	3.2	1.4	8.1	4.5	0.8	0.3	172.5	3.5	2.4	0.025	3.6
	28.03	-90.95	Disint.	70	-910	5.8	10.9	2.6	4.4	2.1	3.1	1.7	0.9	0.4	146.7	20.8	3.4	0.025	5.1
26.9	26.51	-90.88	Disint.	148	-2262	12	14.9	2.9	10.9	6.3	7.5	1.6	1.0	0.5	315.0	63.6	15.1	0.026	22.9
	26.72	-90.72	Disint.	55	-2395	7.1	19.3	2.4	8.1	2.7	9.9	3.8	1.1	0.4	255.0	35.4	4.6	0.036	6.9
26.9	27.9	-90.54	Disint.	40	-1091	4.2	10.7	2.2	4.5	2.4	4.4	1.4	0.8	0.5	161.3	29.5	2.1	0.038	3.2
	27.57	-90.24	Disint.	748	-1404	45	5.4	1.1	0.9	0.5	1.0	0.8	1.1	0.6	55.0	10.8	13.6	0.001	20.6
26.9	27.46	-90.04	Disint.	5509	-2328	167	6.4	0.6	1.1	0.5	1.3	0.6	0.5	0.3	53.8	8.5	97.7	0.000	148.0
	28.01	-89.42	Disint.	1394	-2228	79	6.0	1.1	0.9	0.4	1.6	0.5	n/a	n/a	73.8	7.5	33.9	0.001	51.4
26.9	29.1	-88.93	Disint.	2913	-1136	124	5.5	1.7	1.0	0.6	2.0	1.0	n/a	n/a	48.3	25.7	46.5	0.000	70.4
	29.95	-87.64	Disint.	2460	-1414	110	7.8	1.8	1.0	0.5	1.3	0.6	n/a	n/a	97.5	15.5	79.1	0.001	119.9
26.9	30.87	-87.02	Disint.	1098	-121	89	5.1	0.6	1.9	1.0	1.9	0.5	0.7	0.3	60.0	10.0	13.1	0.001	32.9
	Mean	27.5	-91.0	663.0	-1646.9		11.5		4.0		4.4		1.5		139.9		17.8	0.017	total
26.9	Standard deviation	1.1	1.5	1278.2	555.8		4.4		2.8		3.3		1.5		72.9		30.3	0.017	687.0
	Median	27.4	-91.3	55.0	-1733.0		10.9		3.3		3.1		1.0		146.7		3.4	0.014	
New Jersey	39.29	-72.41	Disint.	62	-1695	21	27.3	6.1	3.3	1.8	3.0	1.1	1.7	1.1	163.3	47.3	3.3	0.008	5.1
	39.21	-72.57	Disint.	52	-1662	16	29.3	5.9	5.1	3.5	4.0	2.5	1.0	0.5	200.0	7.1	3.4	0.013	5.2
<i>n</i> = 13	39.17	-72.61	Disint.	27	-1718	12	24.2	8.3	2.1	1.2	6.3	2.5	5.0	4.1	168.3	23.1	1.5	0.014	2.3
	39.08	-72.6	Slump	44	-1851	8	11.3	2.6	3.8	2.0	3.6	1.7	2.3	0.9	126.7	45.1	1.8	0.016	2.8
Total area: 3040	39.02	-72.79	Disint.	15	-1574	6.5	20.1	2.9	3.2	1.5	5.2	1.5	n/a	n/a	136.7	15.3	0.7	0.021	1.0
	39.02	-72.73	Slump	5	-1782	5.4	13.3	4.3	2.6	1.4	3.6	1.1	3.2	1.2	125.0	24.2	0.2	0.023	0.3
9.5	39.03	-72.76	Disint.	15	-1615	11	13.0	4.3	2.8	1.2	3.2	1.3	3.0	1.7	100.0	28.6	0.5	0.009	0.7
	38.97	-72.84	Disint.	16	-1425	6.9	12.3	3.4	4.3	1.7	4.2	1.7	n/a	n/a	95.0	22.9	0.5	0.014	0.8
9.5	38.96	-72.76	Disint.	14	-1899	8.3	17.7	5.9	4.9	2.7	5.1	2.7	2.7	2.2	125.0	39.1	0.6	0.015	0.9
	38.93	-72.84	Disint.	11	-1629	6.5	15.5	4.5	2.2	1.0	3.2	1.4	3.5	1.1	130.0	10.0	0.5	0.020	0.7
9.5	38.93	-72.79	Disint.	5.4	-1934	2.5	12.8	3.9	3.2	1.3	3.4	0.8	n/a	n/a	140.0	17.3	0.2	0.056	0.4
	38.91	-72.77	Disint.	9.1	-2056	4.6	23.5	4.5	5.0	3.1	3.9	1.8	2.0	1.3	198.3	2.9	0.6	0.043	0.9
9.5	38.86	-72.8	Slump	13	-2149	5.9	10.3	3.0	3.2	1.5	3.9	1.1	2.9	1.4	106.7	30.6	0.5	0.018	0.7
	Mean	39.0	-72.7	22.2	-1768.4		17.7		3.5		4.0		2.7		139.6		1.1	0.021	total
9.5	Standard deviation	0.1	0.1	18.6	203.5		6.5		1.0		0.9		1.1		33.9		1.1	0.014	21.7
	Median	39.0	-72.8	15.0	-1718.0		15.5		3.2		3.9		2.8		130.0		0.6	0.016	

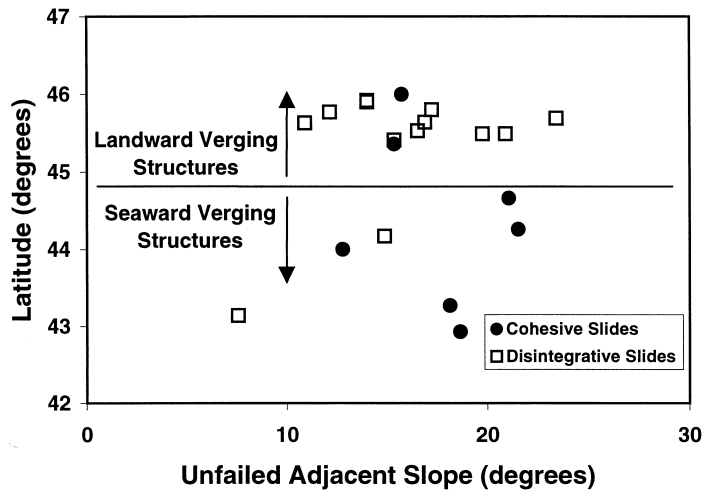


Fig. 9. The unfailed adjacent slope gradient vs. latitude in Oregon. The majority of disintegrative landslides occur in the region of landward verging structures, north of 44.8° . South of 44.8° , most of the landslides are blocky, and there is little change in the slope gradient on which landslides are occurring.

all but two (located on the upper continental slope) are at the toe of the prism, and runoff west.

Most of the landslides offshore central California occur near canyons. Fifteen of the 25 mapped failures occur on the sidewalls of the major canyons or sea-valleys. The headscarps of these landslides tend to sub-parallel to the canyon axis. Four failures occur in a pockmarked region of the upper continental slope in the Point Arena Basin (two in a canyon in the pock marked region; Figs. 2b and 10). Ten landslides occur on the incised slope between the major canyons.

The salt-tectonics-dominated region of the Gulf of Mexico has the lowest mean local slope gradient of the four regions in this study (Pratson and Haxby, 1996), and the largest landslides. There are four provinces where landslides occur in the Gulf: (1) on the steep sidewalls of the salt withdrawal basins; (2) in the low gradient regions between basins; (3) at the base of the Sigsbee Escarpment and (4) adjacent to Mississippi Canyon (Fig. 11). The blocky landslides and slumps all occur within salt withdrawal basins. The very largest landslides in this study occur adjacent to Mississippi Canyon, and in the interbasin regions.

Nine of the 13 landslides on the New Jersey margin occur on the continental slope between Carteret and Lindenkohl Canyons, where there are no major

canyons. The remaining four occur in Middle Toms, Toms, and Hendrickson (2) Canyons.

3.2. Curious morphologies

Several of the landslides in Oregon and California have a curious perched morphology—they are disintegrative, but do not erode the slope to the present basin floor. An example of this type of ‘hanging slide’ is shown in Fig. 5 (slide ‘a’) on the westernmost ridge of the accretionary prism, offshore Oregon. There is a distinct bench ~ 300 m above the basin floor, and a less distinct bench ~ 150 m above the basin floor which decreases in height to the north. Two other landslides on the westernmost ridge have their bases at 80 m (45.62°N , 125.48°W) and 140 m (45.49°N) above the basin floor. There are two landslides further back in the prism that stop 80 m (45.77°N , -125.27°W) and 130 m (45.63°N , -125.33°W) above a slope basin floor. Three failures in California’s Vizcaino Canyon have a similar hanging slide morphology, with their terminations at 250, 280 and 330 m above the canyon floor.

Offshore California, four landslides are immediately downslope of a large pock mark field, which covers over 1000 km^2 in the Point Arena Basin (Fig. 10). In places, pock mark density exceeds 3 per km^2 . They vary in size, with an average diameter of

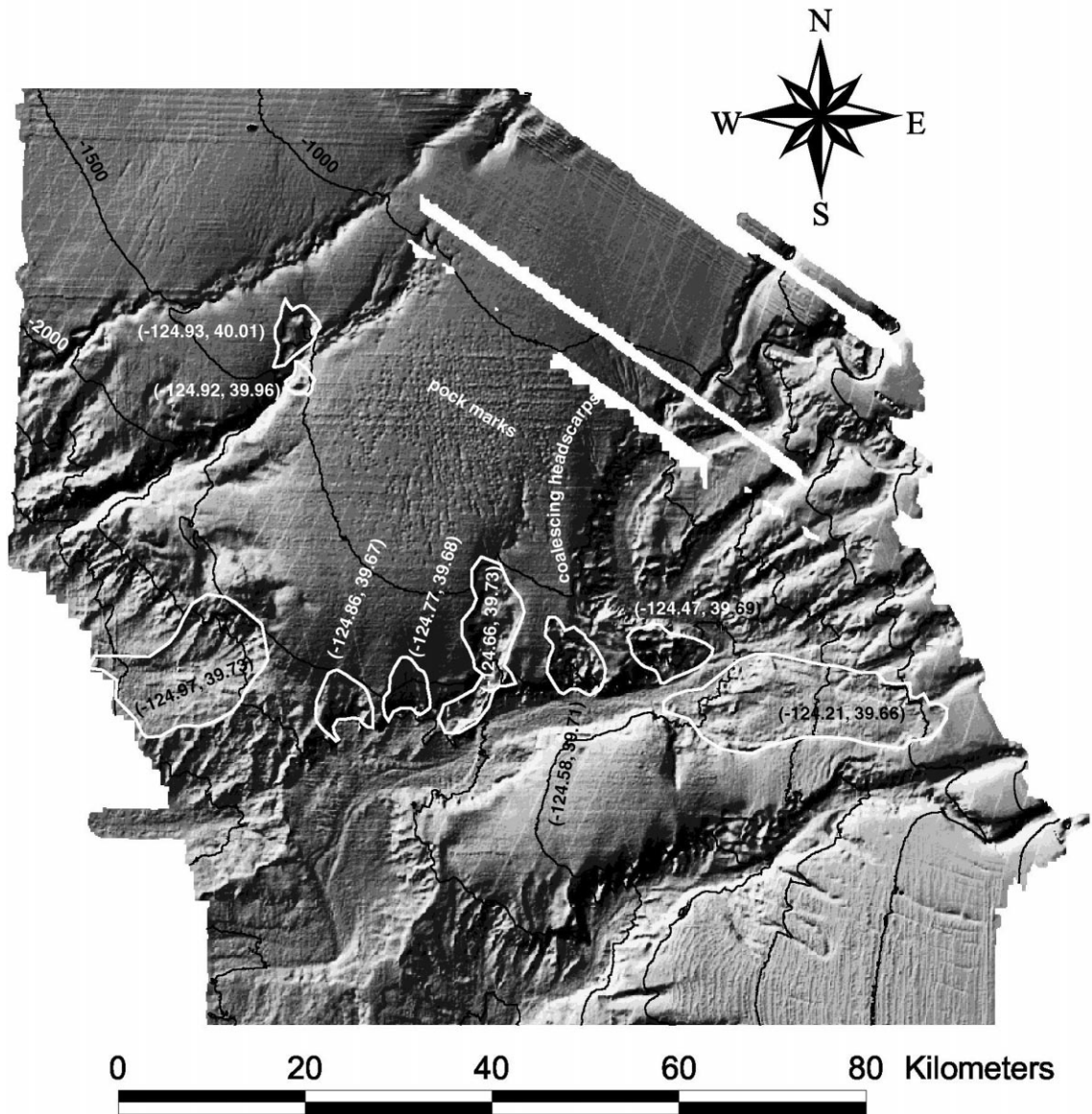


Fig. 10. Northern California margin near Vizcaino Canyon, Point Arena basin (see Fig. 2b for location). The sun illumination angle is low (45° from an azimuth of 315°) to accentuate the pock mark field. Contour interval is 500 m. Vizcaino Canyon is the pitchfork shaped canyon in the lower center of the figure. Note extensive, previously unreported pock mark field north of Vizcaino Canyon. Coalescing pock marks are present in the two northern-most, unnamed channels. An area of coalescing headscarps is present on the western side of a major meander of Vizcaino Canyon, but no individual failures were isolated.

~ 500 m, and can be tens of meters deep. Fig. 10 shows a failure on the north side of Vizcaino Canyon at 39.73°N , -124.66°W , with its headscarp in the pock mark field. In places, the pocks merge together forming a linear, canyon-like depression. Two land-

slides are within channels in the northern portion of the pock mark field, and one in a channel south of the field.

Failures on the sidewalls of Monterey and Vizcaino Canyons show a similar landslide style, where arcuate

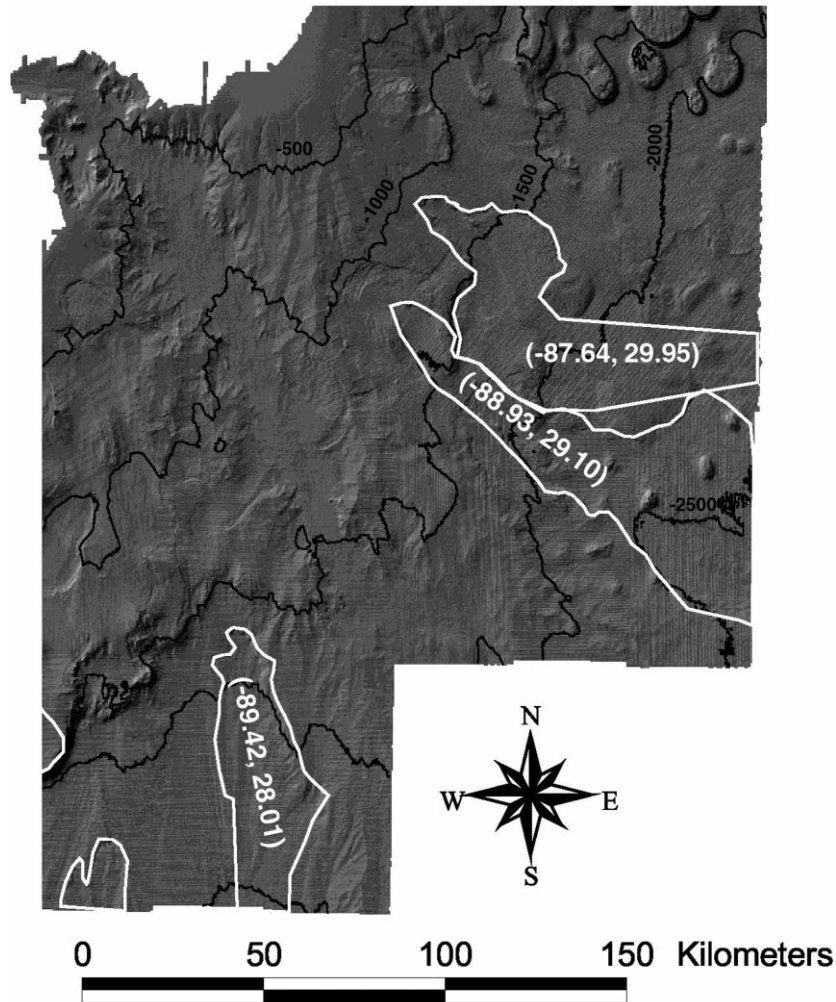


Fig. 11. Large Gulf of Mexico failures, adjacent to Mississippi Canyon (see Fig. 2c for location). Sun illumination angle is 65° from an azimuth of 315° . Contour interval is 500 m. Notice diffuse bathymetry surrounding Mississippi Canyon. The two large landslides northeast of the canyon, cover 2913 and 2460 km^2 , and the one southeast of the canyon is 1394 km^2 . The area measurements are minimums due to the extent of the data. Despite being limited by the data, these landslides are larger than any found in the other study areas.

headscarps coalesce at a given height above the channel base (Figs. 10 and 12). The Monterey Canyon example occurs at 36.24°N , -122.54°W . The headscarps tend to be shallow (<100 m) and are around 1000 m above the canyon floor in each case. The lateral extent of the headscarp stops as the channel of the canyon becomes unconfined. Similar examples occur in the Ascension Sea Valley, where several scarps merge to form 1 scar (Fig. 10). The north side of Vizcaino Canyon shows a great deal of incision and a coalescing headscarp morphology (Fig.

10), but there are no clear and discrete headscarps and/or scarps that fit our criteria. South of Pioneer Canyon, a failure with coalescing headscarps occupies a knoll between two canyons. This landslide complex extends to the canyon base in each direction.

3.3. Slide statistics

In the following section, we review the measurements made on the landslides and their statistics (Table 1). Fig. 13a–d shows histograms of the

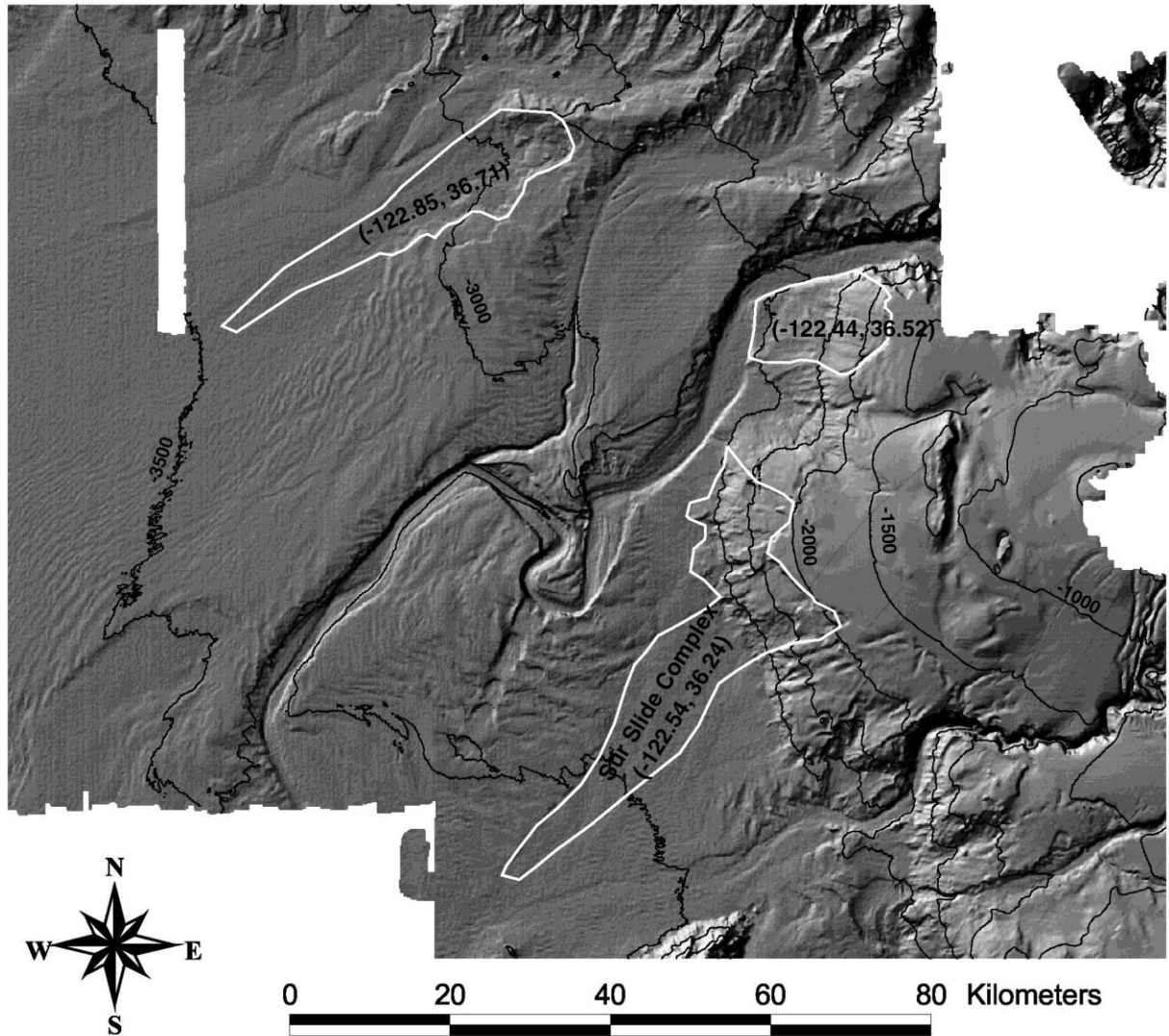


Fig. 12. Monterey Canyon region, offshore central California (see Fig. 2b for location). Sun illumination angle is 65° from an azimuth of 315° . Contour interval is 500 m. The Sur Slide Complex (Normark and Gutmacher, 1988) is an example of a landslide complex with coalescing headscarps that may represent several failures in the same location. The landslides on the south slope of Monterey Canyon ($-122.44, 36.52$), and the one associated with the Ascension Sea Valley ($-122.85, 36.71$) have a coalescing headscarp morphology. This morphology, predicted by Densmore et al. (1997), is created by multiple slope clearing events, each following an episode of canyon incision.

landslide area, depth to headscarp, headscarp height, and local unfailed slope angle. Table 2a–g summarize the correlation coefficients for all of the measured variables on each margin (Table 2a–d), all margins combined (Table 2e), and the disintegrative and cohesive (blocky and slumped) landslides (Table 2f and g).

3.4. Depth and regional slope gradient

Pratson and Haxby (1996) plot the range of seafloor slope gradients with water depth using the same bathymetric datasets. In California, failures are evenly distributed between 800 and 2800 mbsl, with a mean depth of 1828 ± 524 mbsl (Fig. 13b). The steepest

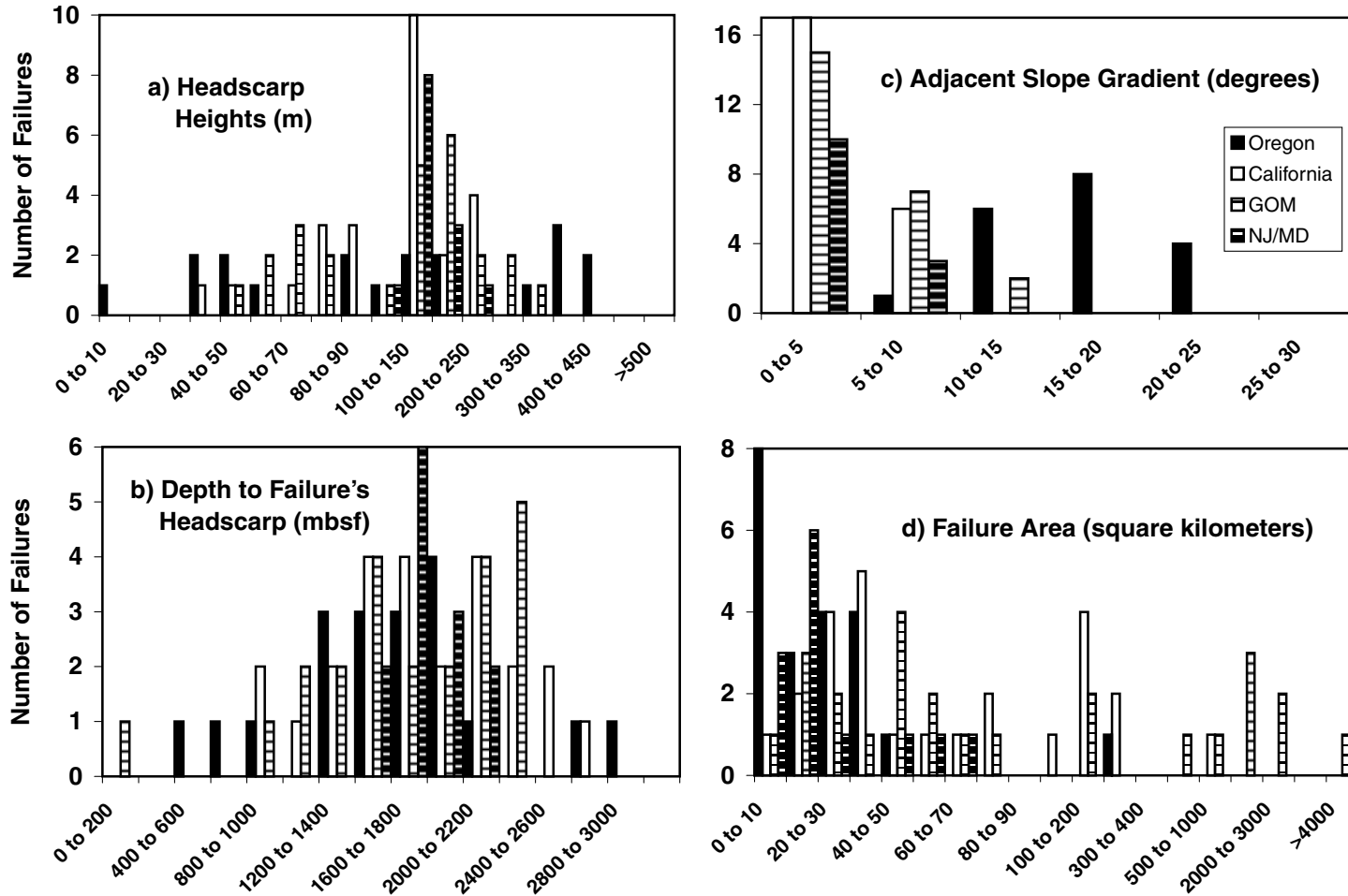


Fig. 13. a–d. Histograms separated by margin. (a) Height of the failure’s headscarp, (b) depth to the headscarp of the failure (in meters below sea level), (c) adjacent slope gradient, which we infer to be similar to the gradient of the slope before it failed, and (d) total area affected by landslide mass. Headscarp heights tend to be higher in Oregon and New Jersey, slightly lower in California, and very low in the Gulf of Mexico, which we interpret to be related to sediment strength (see text). There does not appear to be any systematic trends in depth to the headscarp of the failure, with the exception of the clustering in the mid-depth ranges. The slope adjacent to the failure is very steep in Oregon where most of the failures occur on slope gradients greater than 15°, and very low in the Gulf of Mexico, where most occur on slope angles less than 5°. The Gulf of Mexico has the largest range in failure size, California and New Jersey have a similar area distribution, and the landslides in Oregon tend to be the smallest.

Table 2

a–g. Correlation coefficients. All of the measured and calculated variables are correlated to explore possible relationships. Negative correlations are in italics, and any coefficient greater than or equal to 0.5 is highlighted in bold

	Area	Volume	Runout	Runout slope	HS slope	HS height	Scar slope	LUS	HS depth	D/L
(a) <i>Oregon</i> : OR correlations										
Area	1.00									
Volume	0.99	1.00								
Runout	0.90	0.84	1.00							
Runout slope	<i>-0.19</i>	<i>-0.25</i>	<i>-0.14</i>	1.00						
Headscarp slope	0.11	0.12	0.08	<i>-0.31</i>	1.00					
Headscarp height	0.41	0.47	0.30	<i>-0.30</i>	0.74	1.00				
Scar slope	<i>-0.08</i>	<i>-0.05</i>	<i>-0.17</i>	<i>-0.26</i>	0.61	0.67	1.00			
Local unfailed slope	<i>-0.14</i>	<i>-0.09</i>	<i>-0.15</i>	<i>-0.01</i>	0.75	0.56	0.51	1.00		
Depth to headscarp	0.00	<i>-0.06</i>	0.00	0.37	<i>-0.58</i>	<i>-0.54</i>	<i>-0.37</i>	<i>-0.5</i>	1.00	
D/L	<i>-0.16</i>	<i>-0.08</i>	<i>-0.42</i>	<i>-0.23</i>	0.59	0.63	0.73	0.55	<i>-0.38</i>	1.00
(b) <i>California</i> : Cali correlations										
Area	1.00									
Volume	0.94	1.00								
Runout	0.86	0.80	1.00							
Runout slope	<i>-0.47</i>	<i>-0.48</i>	<i>-0.55</i>	1.00						
Headscarp slope	<i>-0.02</i>	0.08	0.14	<i>-0.14</i>	1.00					
Headscarp height	<i>-0.07</i>	0.16	0.03	<i>-0.39</i>	0.52	1.00				
Scar slope	<i>-0.20</i>	<i>-0.13</i>	<i>-0.28</i>	0.00	0.16	0.17	1.00			
Local unfailed slope	<i>-0.04</i>	0.13	0.03	0.08	0.71	0.42	0.04	1.00		
Depth to headscarp	<i>-0.29</i>	<i>-0.37</i>	<i>-0.34</i>	0.47	<i>-0.38</i>	<i>-0.33</i>	0.04	<i>-0.39</i>	1.00	
D/L	<i>-0.50</i>	<i>-0.40</i>	<i>-0.62</i>	0.21	0.05	0.50	0.43	<i>-0.07</i>	0.10	1.00
(c) <i>Gulf of Mexico</i> : GOM correlations										
Area	1.00									
Volume	0.83	1.00								
Runout	0.96	0.89	1.00							
Runout slope	<i>-0.18</i>	<i>-0.20</i>	<i>-0.20</i>	1.00						
Headscarp slope	<i>-0.52</i>	<i>-0.30</i>	<i>-0.55</i>	<i>-0.05</i>	1.00					
Headscarp height	<i>-0.42</i>	<i>-0.10</i>	<i>-0.43</i>	<i>-0.21</i>	0.85	1.00				
Scar slope	<i>-0.50</i>	<i>-0.50</i>	<i>-0.61</i>	0.01	0.73	0.68	1.00			
Local unfailed slope	<i>-0.41</i>	<i>-0.40</i>	<i>-0.48</i>	0.06	0.78	0.66	0.78	1.00		
Depth to headscarp	<i>-0.14</i>	<i>-0.21</i>	<i>-0.14</i>	0.22	<i>-0.31</i>	<i>-0.33</i>	<i>-0.16</i>	<i>-0.19</i>	1.00	
D/L	<i>-0.49</i>	<i>-0.50</i>	<i>-0.61</i>	<i>-0.10</i>	0.62	0.55	0.64	0.54	0.00	1.00
(d) <i>New Jersey/Maryland</i> : NJ/MD correlations										
Area	1.00									
Volume	0.97	1.00								
Runout	0.87	0.88	1.00							
Runout slope	<i>-0.50</i>	<i>-0.54</i>	<i>-0.32</i>	1.00						
Headscarp slope	0.58	0.72	0.68	<i>-0.32</i>	1.00					
Headscarp height	0.42	0.58	0.37	<i>-0.37</i>	0.87	1.00				
Scar slope	0.21	0.26	0.06	<i>-0.77</i>	0.28	0.33	1.00			
Local unfailed slope	<i>-0.10</i>	<i>-0.06</i>	<i>-0.03</i>	0.53	0.27	0.15	0.01	1.00		
Depth to headscarp	0.21	0.19	0.35	0.12	0.15	<i>-0.18</i>	<i>-0.16</i>	0.06	1.00	
D/L	<i>-0.53</i>	<i>-0.44</i>	<i>-0.67</i>	<i>-0.06</i>	<i>-0.16</i>	0.23	0.07	<i>-0.15</i>	<i>-0.29</i>	1.00

Table 2 (continued)

	Area	Volume	Runout	Runout slope	HS slope	HS height	Scar slope	LUS	HS depth	D/L
(e) <i>All margins combined</i> : all correlations										
Area	1.00									
Volume	0.79	1.00								
Runout	0.93	0.87	1.00							
Runout slope	−0.18	−0.23	−0.24	1.00						
Headscarp slope	−0.31	−0.25	−0.37	−0.15	1.00					
Headscarp height	−0.18	0.00	−0.20	−0.27	0.64	1.00				
Scar slope	−0.27	−0.24	−0.37	−0.17	0.63	0.53	1.00			
Local unfailed slope	−0.25	−0.21	−0.35	−0.16	0.71	0.45	0.80	1.00		
Depth to headscarp	−0.04	0.07	0.00	0.12	−0.30	−0.34	−0.06	−0.08	1.00	
D/L	−0.22	−0.18	−0.35	−0.18	0.56	0.60	0.74	0.64	−0.09	1.00
(f) <i>Cohesive (blocky and slumps)</i> : cohesive slides										
Area	1.00									
Volume	0.95	1.00								
Runout	0.79	0.72	1.00							
Runout slope	−0.35	−0.35	−0.33	1.00						
Headscarp slope	0.09	0.22	−0.03	−0.55	1.00					
Headscarp height	0.28	0.44	0.03	−0.65	0.85	1.00				
Scar slope	−0.11	0.03	−0.30	−0.34	0.87	0.78	1.00			
Local unfailed slope	−0.01	0.16	−0.16	−0.49	0.86	0.75	0.81	1.00		
Depth to headscarp	0.29	0.12	0.29	0.28	−0.51	−0.52	−0.40	−0.50	1.00	
D/L	−0.18	−0.05	−0.47	−0.28	0.75	0.74	0.89	0.70	−0.08	1.00
(g) <i>Disintegrative</i> : disintegrative slides										
Area	1.00									
Volume	0.85	1.00								
Runout	0.93	0.87	1.00							
Runout slope	−0.20	−0.23	−0.26	1.00						
Headscarp slope	−0.37	−0.29	−0.44	−0.01	1.00					
Headscarp height	−0.20	0.01	−0.21	−0.11	0.53	1.00				
Scar slope	−0.38	−0.39	−0.50	−0.10	0.52	0.16	1.00			
Local unfailed slope	−0.28	−0.29	−0.40	−0.03	0.64	0.20	0.84	1.00		
Depth to headscarp	−0.04	−0.11	−0.02	0.13	−0.20	−0.32	0.13	0.09	1.00	
D/L	−0.26	−0.27	−0.41	−0.14	0.46	0.43	0.52	0.59	0.01	1.00

slope angles (where one might expect more failures) occur on the upper continental slope (100–300 mbsl), and the lower slope between 1600 and 2600 mbsl (Pratson and Haxby, 1996). The steeper slopes on the New Jersey margin are on the upper continental slope (<1500 mbsl; Pratson and Haxby, 1996), and the slope failures all occur between 1400 and 2600 mbsl around a mean of 1768 ± 204 mbsl (Fig. 13b). The Texas slope has two zones of higher slope angle, one around 1100 mbsl and the other around 2700 mbsl (Pratson and Haxby, 1996), and the failures are evenly distributed between 600 and

2600 mbsl, with a mean at 1710 ± 466 mbsl. Offshore Oregon, landslides occur on a mean of 1589 ± 601 mbsl within a range of 400–3000 mbsl, despite the tendency for the seafloor to be steeper on the upper continental slope (200–450 mbsl) and in deeper water, around 2200 mbsl (Pratson and Haxby, 1996).

3.5. Area, volume, and runout

The largest slope failures by an order of magnitude occur on the Texas continental slope in the Gulf of Mexico (Fig. 13d). A landslide 125 km southwest of

Mississippi Canyon covers 5509 km² of seafloor. The next largest is 2913 km², 40 km east of Mississippi Canyon (Fig. 11). The mean area is 663 ± 1278 km², compared to 93 ± 115 km² in California, 27 ± 52 km² in Oregon and 22 ± 19 km² offshore New Jersey. The Gulf slope also has the highest percentage of its surface area with failures at 27% of the total 61,670 km². The New Jersey margin has 9.5% of its 3040 km² area occupied by landslides, California 7.1% of its 32,930 km², and only 3% of the 18,430 km² offshore Oregon. The total volume of slope failures mapped offshore Texas is 687 km³, with a mean of 27.5 km³. This is compared to a total volume of 134 km³ offshore California (with a mean of 5.3 km³), 75.6 km³ on the Oregon margin (3.8 km³ per failure), and 21.7 km³ (1.7 km³ per failure) offshore New Jersey.

The very large Gulf of Mexico landslides occur adjacent to Mississippi Canyon and in bathymetrically low, interconnected depressions between salt withdrawal basins (Fig. 2c). On the New Jersey slope, the largest landslides occur within Hendrickson and Toms Canyons (Figs. 2d and 4). The largest landslides on the California slope are on the west-facing sidewalls of Monterey Canyon (525 km²; Fig. 12); the southeast side of a meander of Vizcaino Canyon, where the headwall is less than 5 km from the offshore projection of the San Andreas Fault (208 km²; Fig. 10); and the north side of Ascension Sea Valley (295 km²; Fig. 12). There is only one failure (that meets our selection criteria) larger than 100 km² on the Oregon slope. This failure, north of the Heceta South Fault (239 km²; Fig. 14), is one of only two over 100 km² with blocky rubble at the base in all of the study areas (the other is a 143 km² failure on the Texas slope in a salt withdrawal basin). (A series of massive, continental slope-scale failures documented by Goldfinger et al. (2000) using a combination of surface morphology and reflection seismic data, have surface expressions that cover well over 5000 km² of seafloor.)

Overall, the mean area of disintegrative failures is more than seven times that of the blocky (308 ± 865 km² vs. 42 ± 53 km²), but the median for disintegrative failures (30 km²) is slightly lower than that of blocky landslides (34 km²). Fig. 15 shows the area distribution for both blocky and disintegrative landslides. The volume of the disintegrative land-

slides averages 13.6 km³, compared to the cohesive failures' average of 4.8 km³. The mean runout distance for blocky failures is 9.1 km and for disintegrative failures is 16.5 km. The median runout values are 6.8 and 17.4 km for blocky and disintegrative, respectively.

3.6. Headscarps

The heights of headscarps on each margin are seldom exceed 400 m. The shortest measured headscarp heights are on the order of 10 m, which is close to the vertical resolution of the data (Grim, 1992). Cohesive failures tend to have headscarps steeper and taller (17 ± 8°, 185 ± 115 m) than the disintegrative (16 ± 7°, 128 ± 74 m). Oregon has the highest mean headscarp height at 178 ± 146 m, the Gulf of Mexico and New Jersey margins have a mean headscarp height of 140 ± 73 m and 140 ± 34 m, and California is the lowest at 120 ± 55 m. Mean headscarp gradient is highest in Oregon (23 ± 8°), followed by New Jersey (18 ± 6°), California (14 ± 6°) and the Gulf (12 ± 4°). Slumps tend to have larger headscarp height (*D*) to runout length (*L*) ratios, and blocky landslides tend to have a slightly larger *D/L* ratio than fluid ones (Fig. 16).

3.7. Scar and adjacent slope gradients

The steepest slopes adjacent to the failure scar occur in Oregon at 16 ± 4°, with a mean scar slope angle of 14 ± 7°. This is compared to California's 4 ± 2° (slope adjacent to failure) and 6 ± 2° (scar), the Gulf's 4 ± 3° and 4 ± 3°, and 4 ± 1° and 3 ± 1° for New Jersey. The slopes gradients adjacent to the failure and scar slopes tend to be steeper for blocky (9 ± 7° and 10 ± 8°) than disintegrative failures (7 ± 6° and 6 ± 4°). Fig. 17 shows plots of scar slope vs. adjacent unfailed slope angles for each of the four regions. The scar slope is closest to, but slightly steeper than, the unfailed slope angle in Oregon (*m* = 0.98). Scars resulting from failures on the California continental slope are likely to be significantly steeper than the adjacent unfailed slope (*m* = 0.63). The average scar slope has a tendency to be less steep than the surrounding areas on both the Texas and New Jersey margins (*m* = 1.02 and 1.08, respectively). Overall, scar slopes tend to be steeper than the adjacent slope, but disintegrative

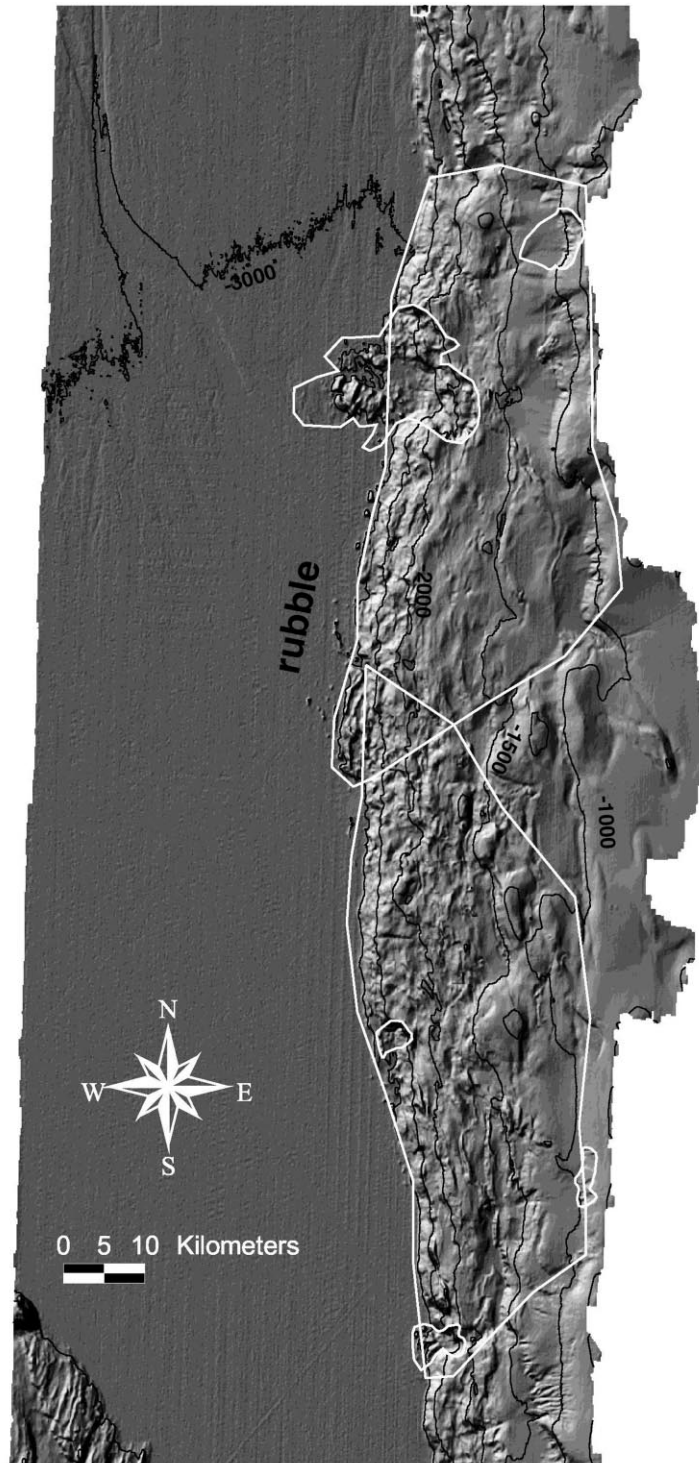


Fig. 14. Super-scale slumps mapped by Goldfinger et al. (2000) on the central Oregon margin. Sun illumination angle is 65° from an azimuth of 315° . Contour interval is 500 m. Because of the large scale of these slumps, our methods could not distinguish the headscarp from the shelf break. Rubble at the base of the continental slope with the lack of a clear headscarps indicates numerous failures with possibly overlapping headscarps.

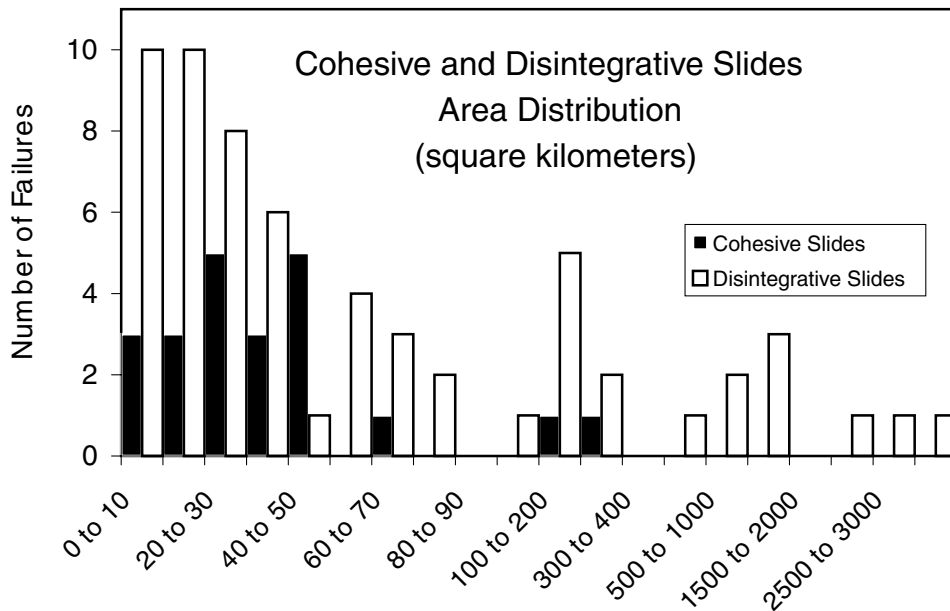


Fig. 15. Area distribution for cohesive and disintegrative landslides. Notice the uneven scale. There are only two cohesive landslides with areas greater than 50 km², whereas the largest disintegrative landslides from the Gulf of Mexico are well over 1000 km².

landslides often have scars less steep than the adjacent slope whereas the scars of cohesive landslides are steeper than the surrounding seafloor (Fig. 18). Fig. 19a and b show that where the unfailed slope angle is lower, landslide area is larger, but only when the runout slope gradients are low.

3.8. Correlations

Table 2a–g list cross-correlations of all morphometric measurements on each margin (Table 2a–d), all margins combined (Table 2e), and cohesive failures (including slumps and those with rubble at the base) and disintegrative landslides overall (Table 2f and g). There is a high correlation between area, volume and runout on all four margins. The headscarp's height and slope gradient also correlate well. Headscarp heights and gradients for failures that maintain post-failure cohesion have a negative correlation with runout slope gradient, but correlate well with D/L . For disintegrative failures (overall and especially on the Texas continental slope), the scar slope has a negative correlation with runout distance. Surprisingly low correlation coefficients include

adjacent slope angle vs. runout distance and runout slope angle to runout distance.

4. Discussion

In this section, we discuss the advantages and limitations of identifying submarine landslides solely from the surface, examine similarities and differences between the failures in this study, and make some inferences about process. Our data agree with Booth et al. (1993) in that slope is not the most important factor in determining where a failure will occur. Sedimentation, erosion, and local geology play a dominant role in determining landslide location and morphology offshore California, Texas, and New Jersey. Tectonics (salt and plate boundary) appears to have significant importance on the Oregon, California, and Texas continental slopes, but does not define a characteristic morphology for a given margin. Sediment rheology probably significantly effects the size of landslides. We also discuss the cumulative effects of multiple landslides on the evolution of a given slope.

The study presents a rapid method of assessing the

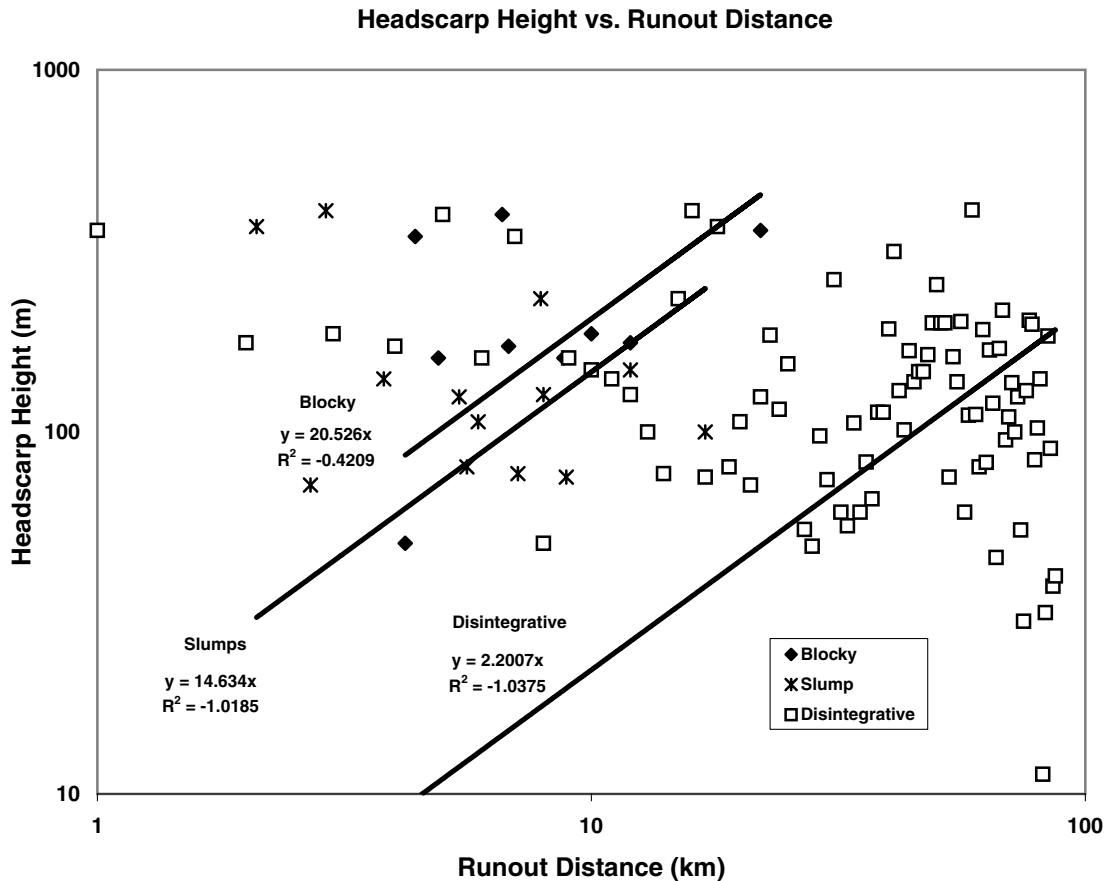


Fig. 16. Headscarp height (D) vs. runout (L) for slumps, and blocky and disintegrative landslides. Linear trend selected on a log–log plot, with intercepts approaching zero. Slumps have the highest D/L ratio (20 m/km) followed by blocky landslides (15 m/km) and disintegrative (2 m/km).

importance of submarine landslides as slope stability indicators and sediment transport mechanisms in the submarine environment. Although we identified over 80 slope failures between the four continental slopes, this study by no means represents a complete catalog of every landslide on each margin. Failures smaller than $\sim 1 \text{ km}^2$ (very large by on-land standards; e.g. Keefer, 1984) are below the resolution of our data. It is possible (and probable) that many small failures ($< 1 \text{ km}^2$) occur throughout these regions, leaving either a smooth appearing, or rough, incised seafloor. These small, overprinting landslides may not leave a distinct landslide signature.

Our measurements overlap with some published slope failures, and vary somewhat because of the different methods of analysis and extent of coverage.

For example, our measurements of the Sur Slide (36.24° , -122.54°) show that the landslide encompasses 525 km^2 of seafloor with a 106 m high headscarp, whereas Normark and Gutmacher (1988) placed the area at $\sim 105 \text{ km}^2$ with a 100-m headscarp. Runout area is difficult to ascertain when net seafloor deposition is spread out over a wide area, and there is little bathymetric or reflective signature. Therefore all runout values are minimums.

Headscarps are often difficult to discern in regions of very rough seafloor such as the southern Oregon and California margins. The landslides we document may represent only a fraction of the total erosion by way of slope failure on each of the continental margins. Based on the slope's rough appearance and the existence of rubble scattered along base of the

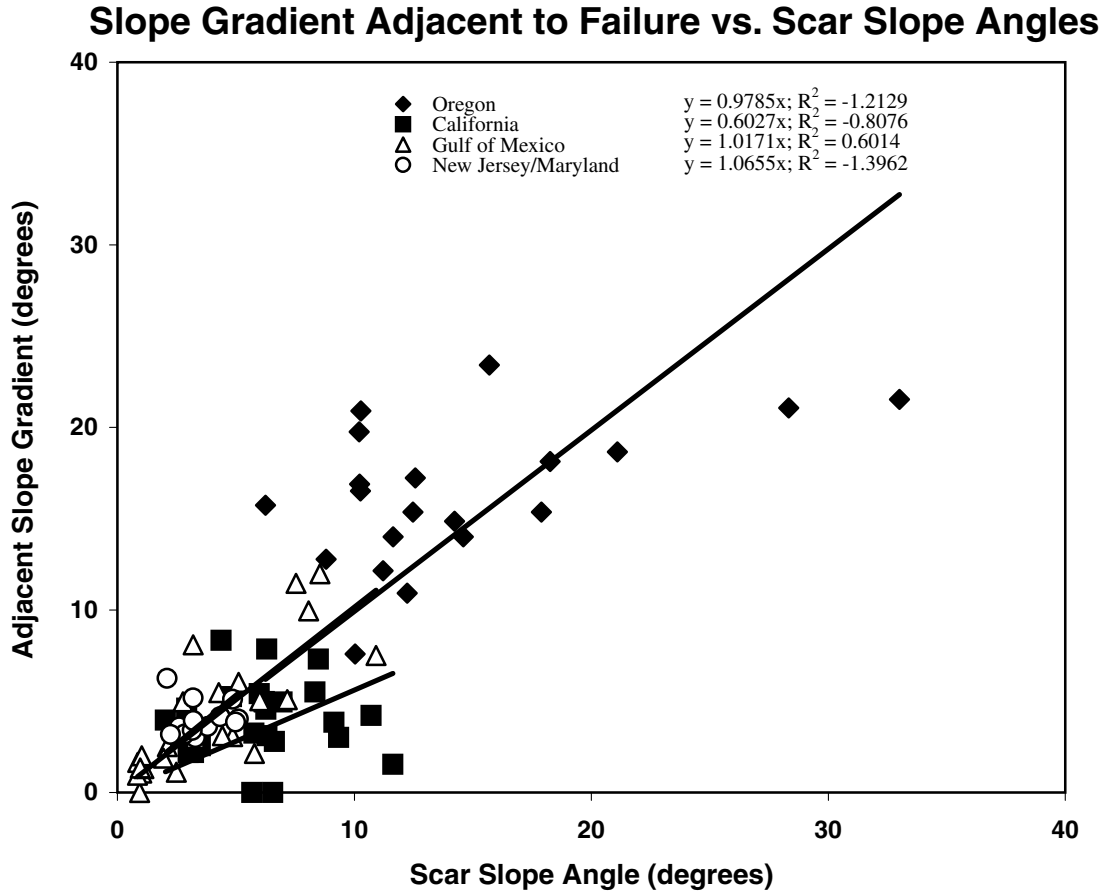


Fig. 17. Slope gradient adjacent to failure vs. scar slope gradient for each of the four regions. When the slope of the trendline is greater than one (the unfailed slope angle is greater than the scar) failures tend to reduce the slope gradient (Gulf of Mexico, New Jersey). If the trendline slope is less than one, then failures tend to make the slope steeper (Oregon, California).

continental slope (Fig. 14), the southern Oregon margin may have had significantly more landslides than the northern margin. Goldfinger et al. (2000) document super-scale slumping in the southern Oregon margin that was not detected using our methods, due to the lack of a distinct headscarp (Fig. 14). California and New Jersey are similar in that inter-canyon slopes tend to have an incised appearance, yet occasional slope failures can be discerned.

Despite the importance of slope gradient in slope stability assessment (Hampton et al. 1996), landslide occurrence does not correspond with *regionally* steep mean slope gradients. Pratson and Haxby (1996) show that slopes tend to be steepest on the upper New Jersey continental slope (<1500 m depth), but the majority

of failures mapped are skewed towards deeper water (Fig. 13b). Similarly, Pratson and Haxby (1996) show that the lower slopes (>2000 m depth) of California and Oregon are steeper, but there is not an obvious increase in landslide frequency below these depths. However, a fair number of failures occur in *locally* steep regions (i.e. the sides of salt withdrawal basins, flanks of anticlinal ridges, or sidewalls of canyons) which represent a small percentage of each continental margin.

If we assume the slope gradient adjacent to the failure is a valid proxy for the pre-failure slope gradient, the majority of failures occur on slopes less than 10° , Oregon being the notable exception where the mean adjacent slope gradient is 16° (Fig. 13c). The

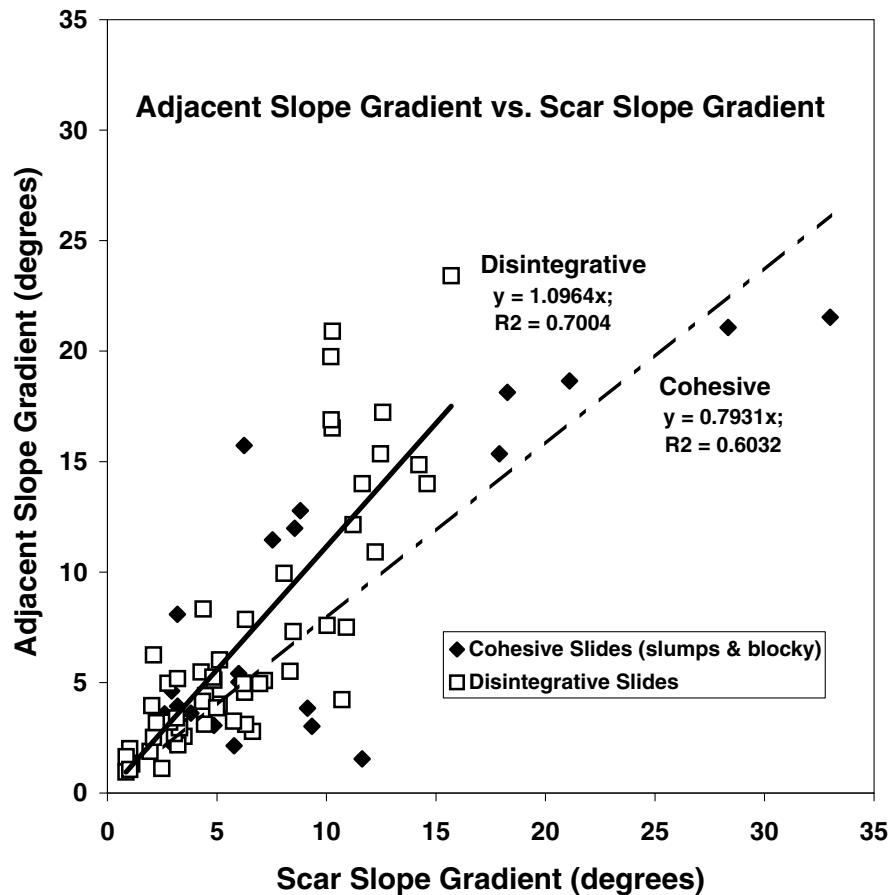


Fig. 18. Graph of the slope gradient adjacent to failure vs. scar slope angle for disintegrative and cohesive landslides. The greater trendline slope for the disintegrative landslides suggests that they tend to make the slope less steep where the cohesive landslides tend to increase the overall slope gradient.

distribution of the adjacent slope for California, Texas and New Jersey is skewed towards the low slope end (Fig. 13c). This suggests that despite having similar regional slope gradient distributions (Pratson and Haxby, 1996), few failures occur on the steep slopes of the California, Texas, and New Jersey margins, whereas few failures occur on the shallower slopes offshore Oregon. Different regions have different processes that control the large slope failures, and slope is not the only controlling factor for failure.

Despite having different tectonic settings, there are several similarities between the California and New Jersey margins that suggest that sedimentation, erosion and local geology are more important controlling factors than is slope. Numerous rills and canyons

erode both continental slopes. The location of landslides on the rilled open slope outside of the major canyons on both the California and New Jersey margins suggests that failure could be influenced by intercanyon down-slope sediment flows that lead to the rills, oversteepening, and subsequent failure as suggested by Pratson and Coakley (1996). Within well-developed canyons, however, the morphology of the landslides is different between the two margins.

The intra-canyon failures of the California and New Jersey margins have markedly different morphologies, which suggest different processes are responsible for the failures. In California, headscarps in Vizcaino and Monterey Canyons trend parallel to the canyon axis, whereas headscarps in Toms and Hendrickson

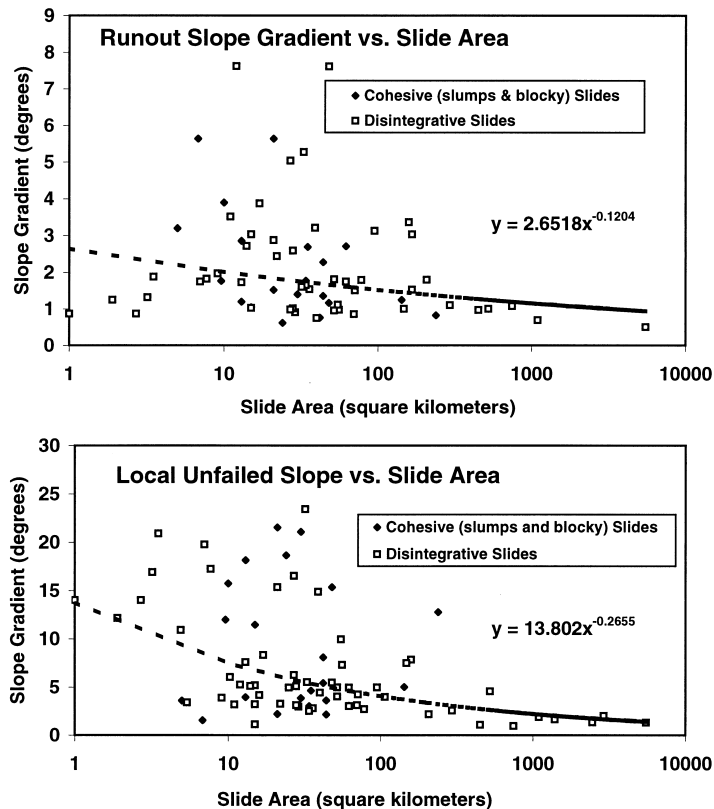


Fig. 19. a and b. Runout and slope adjacent to failure gradients versus landslide area. Squares represent cohesive landslides and circles represent the disintegrative landslides. Trendline is a power-law fit. (a) Semilog plot of runout slope angle vs. landslide area. The very largest landslides are disintegrative and have low-gradient runout zones, and runout zones for cohesive landslides tend to be steeper. (b) Semilog plot of the slope gradient adjacent to the failure vs. the failure's area. The largest landslides occur on low slope angles (less than 5°), whereas a disproportionately high number of the cohesive landslides occur on slope angles greater than 10° .

Canyons on the New Jersey margin are axis-normal. McHugh et al. (1993) suggest that diagenesis and exfoliation of Eocene chinks lead to the observed morphology in Toms and Hendrickson Canyons. The resulting feature resembles a landslide headscarp, but is better characterized as occasional rockfalls that over time erode the canyon headward, but do not cause catastrophic downslope erosive flows (McHugh et al., 1993). The slope-normal headscarps between Carteret and Lindenkohl Canyons are oriented the same way and have the same shape as the Toms and Hendrickson features, therefore suggest that they are most likely due to diagenesis of Eocene chalk, as suggested by McHugh et al. (1993).

The failures in the California canyons are directed towards the canyon axis, rather than parallel, as is the

case in Toms and Hendrickson Canyons. Densmore et al. (1997) present a model of periodic slope-clearing landslides caused by steady canyon incision. As the canyon axis is deepened, slope gradient there increases and undercuts the base of the slope, causing instability. Landslides are directed towards the canyon axis, temporarily filling in the base of canyon. As incision continues, an inner gorge is formed in material from previous landslides. This morphology predicted by the model is similar to the failures found in the California canyons, with an inner gorge and axis-parallel, coalescing failure headscarps, suggesting that canyon incision is responsible for triggering these failures.

This model of canyon incision also helps to explain the "hanging slides" of California's Vizcaino Canyon

(Fig. 10) and Oregon's lower continental slope (Fig. 5). If a failure occurs on the sidewall of a canyon (such as Vizcaino), and this failure erodes to the canyon floor, then over time, further erosion of the canyon floor causes the base of the failure to be perched on the sidewall of the canyon. As long as another slope-clearing event does not occur in the same place, this remnant failure scar will be preserved as a hanging slide. At the base of Oregon's continental slope, the downslope limit of several failure scars corresponds with a bench that can be traced for some distance along the base of the slope (Fig. 5). It is possible that a discrete slope failure event was followed by uplift of the anticlinal ridge, which then raised the base of the scar above the adjoining ocean floor. The benches may represent periods of increased erosion in a channel at the base of the continental slope (Nelson et al., 1970) followed by subsequent uplift above the erosive surface.

The continental slope offshore Texas and Louisiana is markedly different than the other areas, with clearly imaged failures larger by far than all other regions, and slides move, on average, more than five times the volume of sediment. Several factors could aid in producing large failure scars with clear geomorphic signatures. The Gulf of Mexico failures occur where sediment accumulation (rather than erosion) is high (e.g. in the vicinity of Mississippi Canyon, as evidenced by the diffuse topography (Fig. 2c)). Past rapid accumulations of sediment and subsequent salt tectonics may combine to create high fluid overpressures and steep slopes responsible for the inter- and intra-basin failures. Twichell and Delorey (1996) suggest that the lower slope salt withdrawal basins are not as tectonically active as the base of the Sigsbee Escarpment. We found few failures within the basins of the lower slope, but numerous ones in the salt withdrawal basins of the mid- and upper-slope, suggesting that the upper slope basins are more active than the lower slope basins.

The largest slope failures overall are disintegrative, suggesting that either a significant amount of energy caused the failure (i.e. an earthquake; Booth et al., 1993), or that they occurred in weaker material. There are only two cohesive failures greater than 50 km². Fig. 13d shows that the distribution of landslide areas on the Oregon, New Jersey, and California continental slopes is skewed towards the smaller

failures (<30 km²), and decreases in a non-linear fashion. This suggests larger slope failures (>100 km²) are rare on these margins. In the Texas slope data, the less skewed distribution shows that most failures are greater than 30 km², and that larger failures are indeed more common, despite being located far from any locus of seismic activity. The Oregon margin, where large magnitude earthquakes have most likely occurred (Atwater et al., 1991), has relatively few large disintegrative slides. Of the six California landslides between 100 and 500 km², all occur on or near the sidewalls of the large canyons/sea valleys, where erosion and sedimentation are most active. Also, the four landslides near the pockmark field in California's Point Arena Basin may be caused by sediment weakening due to natural gas/fluid venting. Landslides that encompass large areas occur in regions where weaker, perhaps younger, material is present. This suggests a possible explanation as to why the largest slope failures occur in the vicinity of Mississippi Canyon/Fan, where unconsolidated and possibly overpressured material is present, and in the California submarine canyons.

The physics suggests that runout length might increase with the steepness of the pre-failure slope, because a slope of a given height will have higher potential energy on a steeper gradient (Scheidegger, 1973). When all landslides are considered, however, the runout distance is *inversely* related to the steepness of the adjacent slope for each of the margins, except California. This may be because the failures that occur on steeper slopes tend to get spread over a wider area, thus leaving no bathymetric or acoustic signature, and the actual runout is omitted from the measurements. Preferential sediment deposition on shallow slopes provides more weak, erodible material for downslope moving landslides to assimilate. However, failures which occur on steeper slopes change angles rapidly in the runout zone, which may limit the runout. Also, cohesive landslides are less likely to trap overpressured water, which would otherwise aid hydroplaning of the failure (Mohrig et al., 1998).

We use the failures' headscarp morphology to infer sediment strength. Steep headscarps occur in stronger material (Morgenstern, 1967). The cross-correlations show the headscarp's height and slope gradient increase in a predictable fashion with the local unfailed slope angle (Table 2a–g). From this, we

can infer that failures on steeper slopes are often deep seated, whereas those on less steep slopes are thinner. Deep-seated failures will expose more consolidated, stronger material that is less likely to fail.

The continental slope offshore Oregon, where overconsolidation in the accretionary prism is likely, has a large and variable mean headscarp height (178 ± 146 m) with a bimodal distribution. The first mode has a mean height of 83 ± 54 m, and the second, 382 ± 27 m (Fig. 13a). Of the six Oregon landslides in the mode with the higher mean, five are blocky landslides in the seaward vergent section of the southern margin. The single outlier is a large disintegrative failure in the northern landward vergent region, where an entire anticlinal ridge failed from crest to bottom, resulting in a 410 m-high headscarp. Failures in the southern margin tend to be blocky, and have larger headscarps (between 300 and 400 m). Higher headscarps, along with the rough appearance of the southern margin, suggests that the sediment are overconsolidated with a higher strength. Lower headscarp heights (25–100 m) and disintegrative rheologies in the landward vergent region may conversely be the result of weaker, normally consolidated sediment that tend to lose post-failure cohesion (McAadoo et al., 1997).

In the regions other than Oregon, the mean headscarp heights are similar and have a normal distribution (Fig. 13a). California (120 ± 55 m), Texas (140 ± 73 m), and New Jersey (140 ± 34 m) have similar headscarp heights, however the modal values differ slightly. The most common modes of headscarp height for both California and New Jersey are between 100 and 150 m, and Texas, 50–100 m (Fig. 13a). The largest failures on the Texas slope are disintegrative, occur on low slope angles, and correspond to the lower headscarp height mode. The presence of large area failures on very low slope gradients suggests that they have a more fluid rheology during failure, allowing for large runout distances. Again, this may be a result of weak and overpressured near surface sediment that provides a wide, metastable zone for failure (Prior and Coleman, 1982). The higher modal values for headscarp height and smaller failure areas in New Jersey and California may be related to the presence of somewhat stronger, more consolidated material that cannot be as readily eroded during failure as on the Texas slope.

Headscarp height and runout distance have been used together to predict rheology during failure (i.e. rotational slides, viscous or fluid flows, etc.; Crozier, 1973). The ratio of headscarp height (D) to runout distance (L) decreases in low viscosity mass movements. The D/L values for subaerial mass movements range from 21 for rotational slides to 1.6 for flows (Ritter et al., 1995, p. 125). Values measured in this study and others (see Hampton et al. (1996) for a compilation of several studies) range from ~ 0.1 (for slumps) to 0.002. The most viscous submarine landslides tend to move over 10 times further than even the most fluid subaerial landslides. Runout distances in the submarine environment are greater, due in part to the hydroplaning of submarine failed material over smooth surfaces (Mohrig et al., 1998). In their model, Mohrig et al. (1998) show that a layer of lubricating fluid trapped beneath the fronts of advancing subaqueous debris flows, drastically reduces bed drag, and increases head velocity. Regions with low slope gradients where rapid sedimentation has reduced the occurrence of surface roughness are ideal for extremely long runout failures such as those documented around Mississippi Canyon. Fig. 16 shows runout vs. headscarp height for the different rheologies, which allows us to make somewhat reasonable predictions on the runout distance a disintegrative failure might have had based on the headscarp height.

Slope failures may be an important factor in maintaining the overall gradient of the continental slope (Davis et al., 1983). On each of the margins, the mean slope gradient of the scar is similar to the mean slope gradient of the entire continental slope calculated by Pratson and Haxby (1996). The slopes encompassed in the Pratson and Haxby (1996) calculations average steep canyons, chutes, etc. with the lower gradient canyon floors, slope basins, and rigdetops. The similarities are notable in the California ($6.1 \pm 2.5^\circ$ [local unfailed slope] vs. 5.2° [mean local slope]), Texas slope ($4.0 \pm 2.8^\circ$ vs. 2.9°), and New Jersey ($3.5 \pm 1.0^\circ$ vs. 7.6°) margins, with the exception again being Oregon, with the mean slope gradient adjacent to the failure of $14.5 \pm 6.6^\circ$, and the mean local slope gradient of 5.2° (Pratson and Haxby, 1996). When a slope exceeds the critical gradient for a given tectonosedimentary environment, a landslide occurs and the gradient in the scar represents the new stable regime.

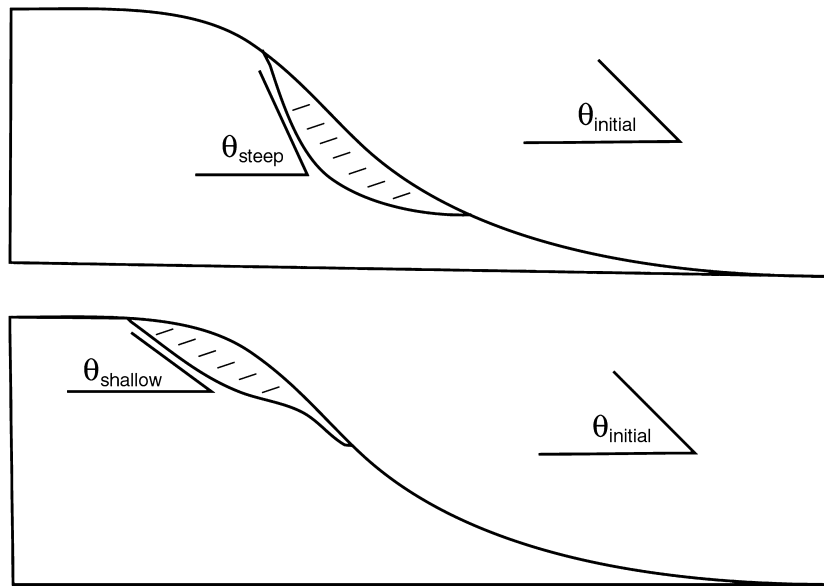


Fig. 20. Cartoon illustration of two possible scar geometries. The scar resulting from a submarine landslide can either be equal to, steeper than, or shallower than the slope on which the failure occurred. If the scar slope angle is steeper than the original, unfailed slope, then over time, repeated landslides of this type tend to make that particular slope steeper. Conversely, if the scar slope has a lower gradient than the initial slope, then landslides can act to reduce the slope gradient in a region.

As landslides expose deeper, more consolidated and stronger material, the nature of the continental slope changes. The resulting scar can be either steeper or shallower than the slope on which the failure occurred (Fig. 20). Separating cohesive and disintegrative failures and examining the scar slope vs. the adjacent unfailed slope shows that in both cases the slope angle of the scar increases with unfailed slope angle, but the final state of the slope (post-failure) tends to be steeper after a cohesive failure (Fig. 18). A landslide in less cohesive material tends to leave a scar that is shallower than the original slope. Over time, multiple cohesive failures tend to make the slope steeper and disintegrative landslides tend to reduce the slope taper (Fig. 20).

The Oregon margin is anomalous when compared to the other three margins. Oregon has a much higher mean slope gradient adjacent to the failure, and a significantly smaller total area affected by failures (Table 1). Many workers have proposed that the Cascadia Subduction Zone is locked between Northern California and Vancouver Island (see review of evidence of Cascadia seismicity in Clague (1997)). Elastic strain may have been released in a series of

magnitude 8 events (McCaffrey and Goldfinger, 1995), or possibly a single event that may have exceeded magnitude 9 (Atwater et al., 1991). In either case, such an event should trigger numerous landslides on the steep lower continental slope. The resulting bathymetry would have a rough appearance, the result of numerous overlapping slope failures, similar to the California margin. The southern, seaward vergent Oregon margin has the rough appearance that one might expect from a seismically active margin, possibly due to numerous overprinted (and hence undetected) failures, as evidenced by the rubble at the base of the slope (Fig. 14). The blocky landslides suggest failure of overconsolidated material. Furthermore, using a combination of bathymetry and seismic reflection data, Goldfinger et al. (2000) suggest a series of potential failures on the southern margin, where almost the entire continental slope collapsed. Despite the evidence of large magnitude earthquakes, the smooth, steep slopes on the landward verging anticlines south of Astoria Canyon remain in many places unfailed and non-eroded (based on sparse landslide occurrence and consolidation tests; McAdoo et al., 1997).

The most commonly called upon trigger for submarine landslides is earthquakes (see USGS Bulletin 2002, 1992), because the deep marine environment lacks transient changes in seafloor conditions associated with weather. Earthquakes remain the most likely failure triggering mechanism in regions such as California and Oregon by default because of their close proximity to seismically active plate boundaries. The large failure on the south side of Vizcaino Canyon (Fig. 2b; 39.66°, -124.47°) is within 5 km of the offshore projection of the San Andreas Fault, and may have been triggered by a seismic event. As previously mentioned, however, large regions of the lower continental slope of Oregon are unfailed, despite their proximity to the Cascadia subduction zone, and the largest disintegrative slides occur in the Gulf of Mexico, far from any seismic activity. Because the New Jersey and Texas margins are far from seismically active regions, failures may be associated with sedimentation events.

It is possible that the slopes in the landward vergent region of Oregon are stable because the weak underlying sediment attenuates seismic energy, and decouples the prism from the subduction plate. Landward vergence requires a weak basal detachment layer (Seely, 1977). Rapid sedimentation associated with the Astoria Fan may yield overpressures on both the basal décollement, and layers within the prism (MacKay, 1995; Goldfinger et al., 2000). If earthquakes occur such as those proposed for the Cascadia plate boundary (see Clague, 1997), weak layers in the accretionary prism may attenuate the high-frequency energy responsible for high accelerations. In the seaward vergent region, basal coupling is likely to be greater, and the observed morphology, including the super-scale slumping documented by Goldfinger et al. (2000), is what one might expect from a large magnitude, plate boundary earthquake. Preliminary results from seismic energy propagation modeling suggest that attenuative media can indeed filter out much of the high frequency (>1 Hz) energy (McAadoo, in preparation).

5. Conclusions

We have gained important insight into submarine processes from the morphometric measurements of 83

submarine landslides on the continental slopes offshore Oregon, California, Texas and New Jersey. Statistics from each margin include the landslide area, runout distance, and headscarp height, along with slope gradients of the runout zone, scar, headscarp, and slope adjacent to the failure. Sedimentation and erosion patterns, along with local geology, are more important factors in controlling landslide size and location than slope and proximity to seismic centers. The largest failures on the Texas and California slopes are in areas of active sedimentation and erosion. Failures in canyons offshore California are probably related to canyon incision, and in places leave hanging slides, where a landslide scar is left perched as the canyon floor is eroded. Failure-like features in the large canyons on the New Jersey margin are related to diagenesis in the local bedrock. Inter-canyon slope failures on the New Jersey and California models have a morphology that agrees with models of downslope sediment flow causing erosion and localized oversteepening. Furthermore, landslides in weaker sediment tend to be larger. Landslides in weaker material have the cumulative effect of making the slope less steep, while the failures in stronger, overconsolidated material make the slope steeper. Tectonics play an important role in the location and size of landslides. Sedimentation and salt tectonics on the Texas slope create locally steep regions on the sides of salt withdrawal basins and at the base of the slope where many failures were observed. A large failure adjacent to the San Andreas Fault may well have been triggered by a seismic event. The southern Oregon margin has evidence that suggests significant seismic activity, but the northern Oregon margin has anomalously smooth sedimented slopes for a seismically active region, perhaps due to attenuation of high-frequency seismic energy by weak prism sediment.

Acknowledgements

This study was funded by the Office of Naval Research under the STRATAFORM program, grants #N00014-96-1-0361 and #N00014-98-1-0503 to D.L.O., and #N00014-97-1-0016 to L.F.P. The Shell Oil Foundation also provides funding for B.G.M. Vassar College has provided invaluable assistance

during B.G.M.'s stay as Minority Scholar-in-Residence. This study was inspired by Homa Lee (USGS), and has benefited tremendously by numerous discussions with him. The manuscript benefited from the thoughtful comments of David Piper, David Twichell, and Chris Goldfinger.

References

- Atwater, B.F., Stuvier, M., Yamaguchi, D.K., 1991. Radiocarbon test of earthquake magnitude at the Cascadia subduction zone. *Nature* 353, 156–158.
- Bea, R.G., 1971. How sea floor slides affect offshore structures. *Oil Gas J.* 69, 88–92.
- Booth, J.S., O'Leary, D.W., Popenoe, P., Danforth, 1993. US Atlantic continental slope landslides; their distribution, general attributes, and implications. In: Schwab, W.C., Lee, H.J., Twichell, D.C. (Eds.). *Selected studies in the US Exclusive Economic Zone*, USGS Bulletin 2002, pp. 14–22.
- Clague, J.J., 1997. Evidence for large earthquakes at the Cascadia Subduction Zone. *Rev. Geophys.* 35, 439–460.
- Coulter, H.W., Migliaccio, R.R., 1966. Effects of the earthquake of March 27, 1964, at Valdez, Alaska, US, Geological Survey Professional Paper, 542-C, 36pp.
- Crozier, M.J., 1973. Techniques for the morphometric analysis of landslides. *Zeitschrift für Geomorphologie* 17, 78–101.
- Dade, W.B., Huppert, H.E., 1998. Long-runout rockfalls. *Geology* 26 (9), 803–806.
- Davis, D., Suppe, J., Dahlen, F.A., 1983. Mechanics of fold-and-thrust belts and accretionary wedges. *J. Geophys. Res.* 88, 1153–1172.
- Densmore, A.L., Anderson, R.S., McAdoo, B.G., Ellis, M.A., 1997. Hillslope evolution by bedrock landslides. *Science* 275, 369–372.
- Dingle, R.V., 1977. The anatomy of a large submarine slump on a sheared continental margin (SE Africa). *J. Geol. Soc. London* 134 (3), 293–310.
- EEZ-SCAN 87, 1991. Scientific Staff, Atlas of the Exclusive Economic Zone, US, Atlantic continental margin, US Geological Survey Miscellaneous Investigations Series I-2054, 174pp.
- Goldfinger, C., Kulm, L.D., Yeats, R.S., Appelgate, B., MacKay, M., Moore, G.F., 1992. Transverse structural trends along the Oregon convergent margin: implications for Cascadia earthquake potential. *Geology* 20, 141–144.
- Goldfinger, C., Kulm, L.D., McNeill, L.C., Watts, P., 2000. Super-scale failure of the southern Oregon Cascadia margin. Keating, B., Waythomas, C. (Eds.). *Pure Appl. Geophys.* (Special Issue on Landslides) (in press).
- Grim, P., 1992. Dissemination of NOAA/EEZ multibeam bathymetric data, NOS. In: Lockwood, M., McGregor, B.A. (Eds.). *1991 Exclusive Economic Zone Symposium; Working Together in the Pacific EEZ Proceedings*, US Geological Survey Circular 1092, pp. 102–109.
- Hampton, M.A., Lee, H.J., Locat, J., 1996. Submarine landslides. *Rev. Geophys.* 34, 33–59.
- Heezen, B.C., Drake, C.L., 1964. Grand Banks slump. *AAPG Bull.* 39, 2505–2514.
- Hughes-Clarke, J.E., 1990. Late stage slope failure in the wake of the Grand Banks earthquake. *GeoMar. Lett.* 10, 69–79.
- Keefer, D.K., 1984. Landslides caused by earthquakes. *GSA Bull.* 95, 406–421.
- Lee, H.J., Schwab, W.C., Booth, J.S., 1993. Submarine landslides: an introduction. In: Schwab, W.C., Lee, H.J., Twichell, D.C. (Eds.). *Submarine Landslides: Selected Studies in the US Exclusive Economic Zone*, US Geological Survey Bulletin 2002, pp. 158–166.
- Lee, H.J., Edwards, B.D., 1986. Regional method to assess offshore slope stability. *J. Geotechn. Engng* 112, 489–509.
- MacKay, M.E., 1995. Structural variation and landward vergence at the toe of the Oregon accretionary prism. *Tectonics* 14, 1309–1320.
- McAdoo, B.G., Orange, D.L., Sreaton, E., Lee, H., Kayen, R., 1997. Slope basins, headless canyons, and submarine palaeoseismology of the Cascadia accretionary complex. *Basin Res.* 9, 313–324.
- McCaffrey, R., Goldfinger, C., 1995. Forearc deformation and great subduction earthquakes: implications for Cascadia offshore earthquake potential. *Science* 267, 856–859.
- McHugh, C.M., Ryan, W.B.F., Schreiber, B.C., 1993. The role of diagenesis in exfoliation of submarine canyons. *AAPG Bull.* 77 (2), 145–172.
- Mohrig, D., Whipple, K.X., Hondzo, M., Ellis, C., Parker, G., 1998. Hydroplaning of subaqueous debris flows. *GSA Bull.* 110 (3), 387–394.
- Morgenstern, N.R., 1967. Submarine slumping and the initiation of turbidity currents. In: Richards, A. (Ed.). *Marine Geotechnique*, University of Illinois Press, Urbana, pp. 189–210.
- Nelson, C.H., Carlson, P.R., Byrne, J.V., Alpha, T.R., 1970. Development of the Astoria Canyon-Fan physiography and comparison with similar systems. *Mar. Geol.* 8, 259–291.
- Normark, W.R., Gutmacher, C.E., 1988. Sur submarine slide, Monterey Fan, central California. *Sedimentology* 35, 629–647.
- Pratson, L.F., Haxby, W.F., 1996. What is the slope of the US continental slope?. *Geology (Boulder)* 24 (1), 3–6.
- Pratson, L.F., Coakley, B.J., 1996. A model for the headward erosion of submarine canyons induced by downslope-eroding sediment flows. *GSA Bull.* 108 (2), 225–234.
- Prior, D.B., Coleman, J.M., 1982. Active slides and flows in under-consolidated marine sediments on the slopes of the Mississippi Delta. In: Saxov, S., Nieuwenhuis, J. (Eds.). *Workshop on Marine Slides and Other Mass Movements*, NATO Conference Series IV Plenum Press, New York, pp. 21–49.
- Ritter, D.F., Kochel, R.C., Miller, J.R., 1995. *Process Geomorphology*, 3rd ed. W.C. Brown Publishers, Boston (p. 125).
- Scheidegger, A.E., 1973. On the prediction of the reach and velocity of catastrophic landslides. *Rock Mechanics* 5, 231–236.
- Schwab, W.C., Lee, H.J., Twichell, D.C., 1993. Submarine landslides; selected studies in the US Exclusive Economic Zone, US Geological Survey Bulletin 2002.

- Seely, D.R., 1977. In: Talwani, M., Pitman, W.C. (Eds.). The significance of landward vergence and oblique structural trends on trench inner slopes, Island Arcs, Deep Sea Trenches, and Back-Arc Basins. American Geophysical Union, Washington, DC, pp. 187–198.
- Twichell, D.C., Delorey, C., 1996. Sedimentary processes in the salt deformation province of the Texas–Louisiana continental slope. In: Gardner, J.V., Field, M.E., Twichell, D.C. (Eds.). *Geology of the United States' Seafloor: the View from GLORIA*, pp. 109–122.